Author Manuscript

Author Manuscript

Author Manuscript

Author Manuscript

HHS Public Access

Author manuscript

Nature. Author manuscript; available in PMC 2020 July 22.

Published in final edited form as:

Nature. 2020 January ; 577(7792): 695–700. doi:10.1038/s41586-020-1947-z.

Mechanism of adrenergic $Ca_V1.2$ stimulation revealed by proximity proteomics

Guoxia Liu[1,*], **Arianne Papa**[2,*], **Alexander N. Katchman**[1,*], **Sergey I. Zakharov**[1,*], **Daniel Roybal**[3], **Jessica Hennessey**[1], **Jared Kushner**[1], **Lin Yang**[1], **Bi-Xing Chen**[1], **Alexander Kushnir**[1], **Katerina Dangas**[1], **Steven P. Gygi**[4], **Geoffrey S. Pitt**[5], **Henry M. Colecraft**[2,3], **Manu Ben-Johny**[2], **Marian Kalocsay**[6,+], **Steven O. Marx**[1,3,+]

[1]Division of Cardiology, Department of Medicine, Columbia University, Vagelos College of Physicians and Surgeons, New York, NY 10032

[2]Department of Physiology and Cellular Biophysics, Columbia University, Vagelos College of Physicians and Surgeons

[3]Department of Pharmacology, Columbia University, Vagelos College of Physicians and Surgeons

[4]Department of Cell Biology, Harvard Medical School, Boston, MA 02115

[5]Cardiovascular Research Institute, Weill Cornell Medical College, New York, NY 10021

[6]Department of Systems Biology, Laboratory of Systems Pharmacology, Harvard Medical School

Increased cardiac contractility during fight-or-flight response is caused by β-adrenergic augmentation of $Ca_V1.2$ channels [1-4]. In transgenic murine hearts expressing fully PKA phosphorylation-site-deficient mutant $Ca_V1.2$ α_{1C} and β subunits, this regulation persists, implying involvement of extra-channel factors. Here, we identify the mechanism by which β-adrenergic agonists stimulate voltage-gated Ca^{2+} channels. We expressed α_{1C} or β_{2B} subunits conjugated to ascorbate-peroxidase [5] in mouse hearts and used multiplexed, quantitative proteomics [6,7] to track hundreds of proteins in proximity of $Ca_V1.2$. We observed that the Ca^{2+} channel inhibitor Rad [8,9], a monomeric G-protein, is enriched in the $Ca_V1.2$ micro-environment but is depleted during β-adrenergic stimulation. PKA-catalyzed phosphorylation of specific Ser residues on Rad decreases its affinity for auxiliary β-

Users may view, print, copy, and download text and data-mine the content in such documents, for the purposes of academic research, subject always to the full Conditions of use:http://www.nature.com/authors/editorial_policies/license.html#terms

[+]Correspondence and requests for materials: Steven Marx, MD, Columbia University, Vagelos College of Physicians and Surgeons, 622 W168th Street, PH-3 Center, New York, NY 10032, 212-305-0271, sm460@cumc.columbia.edu; Marian Kalocsay, PhD, Department of Systems Biology and Laboratory of Systems Pharmacology, Harvard Medical School, 200 Longwood Ave, Armenise 137B, Boston, MA 02115, Marian_Kalocsay@hms.harvard.edu.

[*]equal contribution

Author contributions: Designed research and analyzed data: G.L., A.P., A.N.K., S.I.Z., D.R., J.H., J.K., L.Y., B.X.C., A.K, S.G., G.P., H.C., M.B.J., M.K., S.O.M. Performed research and analyzed data: G.L., A.P., A.N.K., S.I.Z., D.R., J.H., J.K., L.Y., B.X.C., A.K, K.D., G.P., H.C., M.B.J., M.K., S.O.M. Wrote the paper with input from all authors: S.O.M., M.K., H.C., G.P., M.B.J. All authors provided feedback and agreed on the final manuscript.

Competing interests: The authors declare no competing interests.

Data and material availability: All transgenic mice are available from S.O.M. under a material agreement with Columbia University. All data are available in the main text or the supplementary materials. Proteomics raw data and search results were deposited in the PRIDE archive and can be accessed via ProteomeXchange accession: PXD014499, PXD014500, PXD014501. The FRET software is accessible on github: https://github.com/manubenjohny/FACS_FRET

Author Manuscript Author Manuscript Author Manuscript Author Manuscript

subunits and relieves constitutive inhibition of $Ca_V1.2$ observed as an increase in channel open probability. Expression of Rad or Rem, a homolog, also imparted PKA-induced stimulation of $Ca_V1.3$ and $Ca_V2.2$, revealing an evolutionarily conserved mechanism that confers adrenergic-modulation upon voltage-gated Ca^{2+} channels.

The positive inotropic effect of β-adrenergic agonists on the heart is a classical physiological phenomenon universally experienced during excitement, exercise, and fight-or-flight. The effect is mediated by β-adrenergic activation of protein kinase A (PKA) which leads to increased Ca^{2+} influx through L-type $Ca_V1.2$ channels in cardiomyocytes [1-4]. The commonly accepted model is that PKA increases $Ca_V1.2$ current by phosphorylating $Ca_V1.2$ α_{1C}- and/or β_{2B}-subunits (Fig. 1a). However, previously proposed putative regulatory residues on the C-termini of α_{1C} (Ser^{1928}; $Ser/Thr^{1700/1704}$) [10,11] and β_{2B} (Ser^{512} and Ser^{570}) [12] were shown to be dispensable for β-adrenergic stimulation of Ca^{2+} currents in the heart [13-16]. Nevertheless, given multiple other Ser/Thr residues on α_{1C} and β_{2B}, it remained possible that PKA phosphorylation of some combination of these was responsible for β-adrenergic modulation of $Ca_V1.2$ in cardiomyocytes. As shown next, this also is not the case.

Core $Ca_V1.2$ channel subunit phosphorylation is not required for adrenergic regulation

We developed a transgenic approach that enables doxycycline-inducible expression of FLAG- tagged, dihydropyridine (DHP)-resistant $Ca_V1.2$ channels in mice (Fig. 1b) [16]. The transgenic and endogenous $Ca_V1.2$ currents are distinguishable by application of nisoldipine, a Ca^{2+}-channel DHP-antagonist [16]. We mutated all 51 of both conserved and non-conserved Ser and Thr residues within the 35 intracellular PKA consensus phosphorylation sites of rabbit α_{1C} to Ala ("35-mutant α_{1C}"; Extended Data Fig. 1a). In cardiomyocytes, the nisoldipine-insensitive 35-mutant Ca^{2+} currents were both up-regulated and activated at more negative potentials in response to isoproterenol or forskolin, to the same extent as were the pseudo-WT (pWT) α_{1C} channels (Fig. 1c-d; Extended Data Fig. 1b-c).

Similarly, we mutated to Ala all 37 conserved and non-conserved Ser and Thr residues within 28 PKA-consensus phosphorylation sites of human β_{2B} ("28-mutant β_{2B}"; Extended Data Fig. 1d). Cardiomyocytes expressing GFP-tagged 28-mutant β_{2B} (Extended Data Fig. 1e-f) displayed isoproterenol or forskolin-induced stimulation of $Ca_V1.2$ current amplitude (Fig. 1e, g), and a hyperpolarizing shift in the voltage-dependence of activation (Extended Data Fig. 1b), similar to cardiomyocytes isolated from transgenic mice expressing GFP-tagged WT β_{2B} [17].

Finally, we crossed 35-mutant α_{1C} with 28-mutant β_{2B} transgenic mice. Anti-FLAG antibody immunoprecipitation indicated GFP-tagged 28-mutant β_{2B} subunits dominate in the 35-mutant α_{1C} complex (Extended Data Fig. 1g) in cardiomyocytes isolated from these mice. These mutant channels also displayed a normal isoproterenol- or forskolin-induced increase in peak Ca^{2+} current (Fig. 1f-g) and a hyperpolarizing shift in the V_{50} of activation

Author Manuscript Author Manuscript Author Manuscript Author Manuscript

(Extended Data Fig. 1b). These results indicate that β-adrenergic stimulation of $Ca_V1.2$ does not involve direct phosphorylation of α_{1C} or β_2 subunits.

Identifying the $Ca_V1.2$ proteome subdomain

Given the foregoing results, we adapted for application to cardiomyocytes an enzyme-catalyzed proximity labeling method [5,6] to comprehensively identify components of the $Ca_V1.2$ macromolecular complex. We generated transgenic mice with doxycycline-inducible, cardiomyocyte-specific expression of DHP-resistant-α_{1C} or β_{2B} proteins with ascorbate-peroxidase (APEX2) and a V5 epitope conjugated to the N-termini, enabling biotin-labeling of proteins within ~20 nm [18] of the Ca^{2+} channels. Fusing APEX2 to α_{1C} and β_{2B} did not affect $Ca_V1.2$ subcellular localization and function in cardiomyocytes assessed using cellular electrophysiology, fractional shortening and immunofluorescence (Extended Data Fig. 2a-d). Incubating isolated ventricular cardiomyocytes or perfusing whole hearts with a solution containing biotin-phenol followed by exposure to H_2O_2 induced robust biotinylation of proteins in a striated z-disk pattern coinciding with the pattern of transgenic α_{1C} and β_{2B} subunits (Fig. 2a-b; Extended Data Fig. 2d-e).

Western blots confirmed biotinylation of proteins known to be localized near $Ca_V1.2$ at dyadic junctions in cardiomyocytes (Fig. 2c). By contrast, $K_V1.5$ channels were not biotinylated and enriched (Fig. 2c), implying that these channels may not be as closely localized to $Ca_V1.2$. Triple-stage mass spectrometry (TMT SPS MS^3) identified and quantified hundreds of other biotinylated proteins (Supplementary Data Table 1), although many likely constitute bystanders rather than physically interacting proteins. Of these, the 150 proteins with the highest peptide-counts were remarkably similar for α_{1C}-APEX2 and β_{2B}-APEX2 transgenic mice (Extended Data Fig. 3a). These were primarily classified as being membrane, cytoskeletal, and sarcomeric proteins (Extended Data Fig. 3b-c, Supplementary Data Table 2). Some of these proteins, however, were associated with other compartments likely reflecting the labeling of proteins encountered during $Ca_V1.2$-APEX2 synthesis, maturation, and trafficking.

Isoproterenol-induced changes in $Ca_V1.2$ neighbors

It seemed likely that PKA-dependent stimulation of Ca^{2+} current in the heart involves recruitment of a distinct activator protein to, or loss of an inhibitory protein from, the $Ca_V1.2$ macromolecular complex. Recently, APEX2-labeling, combined with either multiplexed quantitative mass spectrometry [7] or quantitative proteomics using a system of spatial references and bystander ratio calculations [19], was utilized to analyze ligand-induced changes in the local environment of G-protein-coupled receptors. Importantly, conjugation of the peroxidase to either of the $Ca_V1.2$ subunits did not interfere with β-adrenergic stimulation of Ca^{2+} currents (Extended Data Fig. 2f-g), and the β-adrenergic agonist signaling pathways were preserved in the presence of biotin-phenol and during H_2O_2-induced labeling, assessed by phospholamban phosphorylation (Extended Data Fig. 2h-k).

Isolated cardiomyocytes from α_{1C}-APEX2 and β_{2B}-APEX2 mice were pre-incubated with biotin-phenol for 30-minutes, and during the final 10-minutes, also exposed to either

Author Manuscript Author Manuscript Author Manuscript Author Manuscript

isoproterenol or vehicle (Fig. 2d). Biotinylated proteins were purified and quantified using TMT SPS MS^3. Relative summed peptide TMT signal-to-noise, indicating relative protein quantification, changed for several proteins (Fig. 2e-f). We also probed the effect of isoproterenol on the $Ca_V1.2$ proteome signature in Langendorff-perfused whole hearts (Fig. 2g-h). Isoproterenol-induced recruitment of the PKA catalytic subunit (PKA_{cat}) to $Ca_V1.2$ channels was detected in cardiomyocytes isolated from both α_{1C}-APEX2 and β_{2B}-APEX2 mice (Fig. 2e-f). All three approaches (isolated cardiomyocytes from α_{1C}-APEX2 and β_{2B}-APEX2 mice, and α_{1C}-APEX2 whole hearts) indicated a 30-50% decrease in the amount of the small Ras-like G-protein, Rad, following application of isoproterenol (Fig. 2e-f,h, Extended Data Figs. 4a-c, 5a-b, Supplementary Data Tables 3-5). Analyzing the overlap of proteins displaying isoproterenol-induced changes in α_{1C}-APEX2 and β_{2B}-APEX2 experiments, Rad was the only candidate protein displaying this behavior (Extended Data Fig. 5b-c). In contrast, a 10-minute exposure of cardiomyocytes isolated from non-transgenic mice to isoproterenol (Fig. 2i) had a minimal effect on proteins relatively quantified by TMT SPS MS^3 and specifically no significant effect on the amount of Rad as compared to non-treated paired cardiomyocytes (Fig. 2j, Extended Data Fig. 4d, Supplementary Data Table 6). In this control experiment, proteins were not proximity labeled. Thus, β-adrenergic stimulation depletes Rad from the neighborhood of $Ca_V1.2$, but not from the cell as a whole.

Rad is a member of the Rad, Rem, Rem2, and Gem/Kir (RGK) family of Ras-like GTP-binding proteins, known for their capacity to inhibit all high-voltage-activated Ca^{2+} channels [8,9], and is a potential PKA target [20]. Moreover, Rad-knockout mice display an increased basal Ca^{2+} current and the Ca^{2+} channels activate at lower voltages, mimicking the effects of β-adrenergic receptor stimulation [21,22]. Other studies, however, led to expectations that Rad is not directly involved in adrenergic regulation of $Ca_V1.2$ since over-expression of Rad [23] or Rem [24] in cultured cardiomyocytes markedly attenuated basal $Ca_V1.2$ current that was not rescued by β-adrenergic stimulation. Nevertheless, our proximity labeling results elevated Rad as the leading candidate for the critical missing link that enables PKA regulation of $Ca_V1.2$.

PKA regulation of $Ca_V1.2$ requires phosphorylation of Rad

The robust heterologous reconstitution of PKA regulation of $Ca_V1.2$ currents has been long pursued as a crucial step in identifying and validating the mechanism. We now find that Rad was the missing ingredient. To prove this experimentally, we co-expressed Rad with α_{1C} and β_{2B} subunits in HEK293T cells, limiting Rad expression by using 1:3 to 1:6 cDNA ratio of Rad:$Ca_V1.2$ subunits in order to avoid eliminating the Ca^{2+} current. Perforated, whole-cell patch clamp was used to preserve the normal intracellular milieu and signaling cascades, and minimize current run-down. In HEK293T cells transfected with only α_{1C} + β_{2B}, superfusion of forskolin over 1-3 minutes had no impact on Ba^{2+} current (Fig. 3a-b, g-h). In contrast, applying forskolin to cells expressing α_{1C} + β_{2B} + Rad increased the maximal conductance (G_{max}) by as much as 4.5-fold and by a mean of 1.5-fold, and shifted the V_{50} for activation (Fig. 3c-d, g-h; Extended Data Fig. 6a-b). The forskolin-induced increase in current was inversely proportional to the basal current density, as observed in cardiomyocytes (Extended Data Figs. 1c, 6c). In HEK293T cells expressing 35-mutant α_{1C} + 28-mutant β_{2B} + Rad,

Author Manuscript Author Manuscript Author Manuscript Author Manuscript

applying forskolin increased G_{max} by as much as 3.1-fold and by a mean of 1.9-fold, and caused a hyperpolarizing shift in the V_{50} for activation (Fig. 3i, Extended Data Fig. 6d-e). For both WT and phospho-site mutant α_{1C} and β_{2B} subunits, the forskolin-induced enhancement of Ba^{2+} current in Rad-transfected cells was greatest at hyperpolarized potentials and fell as the test potential approached the reversal potential (Extended Data Fig. 6f-g), consistent with observations in cardiomyocytes [25].

We used single-channel recordings to determine the mechanism of PKA/Rad modulation of $Ca_V1.2$. In the absence of Rad, sweeps with no openings or blank sweeps are rare, while most sweeps exhibit either intermediate or high levels of openings (Fig. 3j, Extended Data Fig. 6h, k). In HEK293T cells transfected with α_{1C} + β_{2B}, co-expression of PKA_{cat} subunit had no effect on open probability (P_O) (Fig. 3j). When Rad is expressed, the fraction of blank sweeps is increased, low activity mode predominates, and the P_O is reduced (Fig. 3k, Extended Data Fig. 6i). By comparison, if the PKA_{cat} subunit is co-expressed with Rad, the fraction of blank sweeps is reduced, the high activity mode resurges, and P_O is increased by 10.6 ± 2.9-fold compared to transfection without PKA (Fig. 3k, Extended Data Fig. 6j, l). These results suggest that Rad potently dampens $Ca_V1.2$ current while phosphorylation of Rad allows channels to operate as though they were devoid of Rad.

We identified 14 consensus PKA phosphorylation sites in Rad (Extended Data Fig. 7a), which were mutated to Ala. This mutant Rad effectively inhibited $Ca_V1.2$ currents; however, the cAMP-PKA mediated upregulation of $Ca_V1.2$ current was lost (Fig. 3g). In lysates from forskolin-stimulated HEK293T cells transfected with GFP-Rad, we observed phosphorylation of Ser^{25}, Ser^{38} and Ser^{300} by mass spectrometry (Extended Data Fig. 7b). These residues were previously identified in the hearts of mice as phosphorylation targets [26] (Extended Data Fig. 7c). We were unable to detect either non-phosphorylated or phosphorylated peptides containing Ser^{272}, notwithstanding prior biochemical studies identifying Ser^{272} as a PKA target [20]. Alanine-substitutions of Rad at Ser^{25}, Ser^{38}, Ser^{272} and Ser^{300} (4-SA mutant, Extended Data Fig. 7d) prevented the forskolin-induced increase in G_{max} and hyperpolarizing shift in the I-V curve (Fig. 3e, g-h). In contrast to transfection with WT Rad, co-transfection of PKA with 4-SA mutant Rad failed to increase P_O (PKA to no PKA: 1.15 ± 0.56-fold; Fig. 3l).

A C-terminal polybasic region of 32 amino acids in Rad is involved in plasma membrane targeting via binding to negatively charged phospholipids such as phosphatidylinositol 4,5-bisphosphate ($PI(4,5)P_2$ or PIP2) [27]. Deletion of the C-terminus of RGK GTPases prevents their inhibition of Ca^{2+} channel function [9]. We found that Ala-substitutions at Ser^{272} and Ser^{300} (2-SA mutant) within the C-terminal polybasic membrane region prevented both the forskolin-induced increase in current amplitude and the hyperpolarizing shift in the I-V curve (Fig. 3f-h; Extended Data Fig. 6c).

Rad binding to β is required for PKA regulation of $Ca_V1.2$ channels

Rad can inhibit $Ca_V1.2$ via β-dependent and β-independent (α_{1C}-dependent) mechanisms [28]. Either Ala-substitutions of Rad at residues R208 and L235, or Ala-substitutions at residues D244, D320 and D322 of β_{2B} (Extended Data Fig. 8a-b) attenuate Rad binding to β

Author Manuscript Author Manuscript Author Manuscript Author Manuscript

subunits [28,29]. These mutations prevented the forskolin-induced increase in G_{max} and the hyperpolarizing shift in the I-V curve (Fig. 4a; Extended Data 8c-d). Thus, the Rad-β subunit interaction is essential for cAMP-PKA regulation of $Ca_V1.2$.

We utilized flow-cytometry Förster resonance energy transfer (FRET) 2-hybrid assay [30] to probe potential PKA-mediated changes in the binding of β_{2B} subunit and WT Rad. At baseline, robust binding is detected between Cerulean-tagged β_{2B} subunit and Venus-tagged WT Rad, consistent with previous studies [31] ($K_{d,EFF}$ = 7957 ± 418; Fig. 4b, Extended Data Fig. 9c). Co-expression of PKA_{cat} subunit, however, markedly weakened this interaction ($K_{d,EFF}$ = 145231 ± 3084). In contrast, co-expression of the PKA_{cat} subunit in cells expressing fluorophore-tagged β_{2B} and 4-SA mutant Rad had no effect on FRET binding ($K_{d,EFF}$ = 4349 ± 138 versus $K_{d,EFF}$ = 4346± 197 with and without PKA catalytic domain respectively; Fig. 4c, Extended Data Fig. 9c). These results suggest that phosphorylation of Rad is required for dissociation of the Rad-β_{2B} interaction. In a similar manner, PKA phosphorylation of Rad also reduced FRET binding to both β_3 and β_4 (Extended Data Fig. 9a-c).

Rad and Rem confer PKA regulation to $Ca_V1.3$ and $Ca_V2.2$ channels

In adrenal chromaffin cells and the sinus node cells of the heart, L-type $Ca_V1.3$ channels are robustly stimulated by PKA [32,33]. In HEK293T cells transfected with only $Ca_V1.3$ α_{1D} + β_{2B}, superfusion of forskolin over 1-3 minutes had no impact on Ba^{2+} current (Fig. 4d-f). In contrast, in cells expressing α_{1D} + β_{2B} + Rad, applying forskolin increased G_{max} by as much as 2.3-fold and by a mean of 1.9-fold, and shifted the V_{50} for activation (Fig. 4d-f). We also expressed the N-type $Ca_V2.2$ α_{1B} subunit, which is widely expressed in neurons, with β_{2B} and Rad in HEK293T cells. Forskolin increased G_{max} through $Ca_V2.2$ when co-expressed with Rad by a mean of 2.2-fold and shifted the V_{50} for activation (Fig. 4g-i). For both $Ca_V1.3$ and $Ca_V2.2$, attenuating binding of Rad to β prevented the forskolin-induced modulation of $Ca_V2.2$ current (Extended Data Fig. 8e-f). We also expressed in HEK293T cells the $Ca_V2.2$ α_{1B} subunit with β_{2B} and Rem, another member of the RGK GTPase family. Forskolin increased G_{max} through $Ca_V2.2$ when co-expressed with Rem by 1.6-fold and shifted the V_{50} for activation (Fig. 4g-i). Thus, PKA-modulation of Ca_V channels is not idiosyncratic as currently believed; rather, it is emerging to be a universal mechanism transferable to all Ca_V channels that bind β subunits.

Discussion

The core α_{1C} and β_{2B} subunits, previously hypothesized to contain the PKA target sites required for β-adrenergic agonist-induced stimulation of $Ca_V1.2$, do not. Rather, successful reconstitution of regulation in a heterologous expression system required an additional component, which we now identify as Rad. The cAMP-PKA regulation on $Ca_V1.2$ required both the phosphorylation by PKA on the C-terminus of Rad and the interaction of Rad with the β subunit. Multiple-alignment analysis of mouse Rad and other species shows conservation of the four phosphorylation sites (Extended Data Fig. 10a). The required interaction with the β subunit is consistent with our recent findings showing that disrupting the α_{1C}-β interaction prevented PKA regulation of $Ca_V1.2$ in heart [17].

Author Manuscript Author Manuscript Author Manuscript Author Manuscript

Analysis of Rad and other members of the RGK GTPase family indicate that their C-terminal phosphorylation sites are highly similar (Extended Data Fig. 10b). Short stretches of basic and hydrophobic amino acids are known to interact with the membrane [27] and phosphorylation of residues within these stretches alters their electrostatic character, thereby reducing membrane affinity. [34] We found that phosphorylation of two Ser residues within the C-terminal polybasic region of Rad released the Ca^{2+} channels from Rad-mediated inhibition, likely mediated by reducing the affinity of Rad with the membrane and the $Ca_V\beta$-subunit (Fig. 4j-k). This mechanism of regulation is modular and transferable as $Ca_V1.3$ channels and neuronal $Ca_V2.2$ channels are also imparted with forskolin-PKA mediated upregulation by Rad and Rem. The activation of Ca^{2+} channels via release of inhibition by PKA phosphorylation is reminiscent of PKA phosphorylation of phospholamban, an inhibitor of SERCA [35].

Whereas phosphorylation of Ser^{1928} is definitively not required for β-adrenergic regulation of $Ca_V1.2$ in the heart, Ala-substitution of Ser^{1928} prevents β-adrenergic stimulation of Ca^{2+} channels in hippocampal neurons and hyperglycemia-induced stimulation of Ca^{2+} currents in arterial smooth muscle cells [36,37]. Perhaps, there are tissue-specific differences in $Ca_V1.2$ regulation. Phosphorylation on the α_{1C} subunit may also affect the trafficking and channel clustering in neurons and cardiomyocytes [38,39].

Our results indicate that proximity labeling using APEX2 is feasible in heart and combined with multiplexed TMT proteomics can identify a dynamically evolving network of interactions induced by β-adrenergic stimulation. This study establishes the utility of proximity labeling in animals and provides an important foundation for future studies that will investigate how diseases, such as heart failure, change the proteomic subdomain of the excitation-contraction coupling machinery.

Augmented Ca^{2+} entry loads the cardiomyocyte with additional Ca^{2+} and enhances RyR opening via Ca^{2+}-induced Ca^{2+} release. This increases cardiac contractility. Dysregulation of $Ca_V1.2$ activity can result in cardiac arrhythmias, heart failure and sudden death. Supporting an important role of RGK GTPases in humans, a Rem2 variant was identified as a genetic modifier in long QT syndrome 2 [40], and a Rad variant was recently linked to Brugada syndrome [41]. Our results identify potential targets and interaction sites for the therapeutic modulation of β-adrenergic regulation of Ca^{2+} currents in the heart and other tissues. For instance, disrupting the interaction between Rad and β subunit can be inotropic by increasing Ca^{2+} entry in the heart. Conversely, interfering with the α_{1C}-β interaction [17], blocking PKA phosphorylation of Rad or potentially enhancing the interaction of Rad with the plasma membrane could attenuate the sympathetic nervous system activation of cardiac Ca^{2+} entry and inotropy more specifically than achievable with β-blockers.

Methods:

Clone construction and cell culture.

All mouse N-terminal-GFP-tagged mouse Rad (accession # XM_006531206) constructs in a pEGFP-C1 vector were generated by gene-synthesis (Gene Universal). The human $Ca_V2.2$ (pSAD442-1) was a gift from Diane Lipscombe (Addgene plasmid # 62574; http://n2t.net/

Author Manuscript Author Manuscript Author Manuscript Author Manuscript

addgene:62574 ; RRID:Addgene_62574). All cDNA clones were authenticated by sequencing.

HEK293T cells (ATCC, CRL-3216) were cultured in DMEM with 10% FBS, 1% Pen/Strep, and transfected with 3 μg rabbit α_{1C} (accession # X15539) or human α_{1B} (for $Ca_V2.2$ experiments) or rat α_{1D} (for $Ca_V1.3$ experiments, accession # AF3070009), 3 μg human β_{2B} (NM-201590.3) and 0.5 μg N-terminal-GFP-tagged mouse Rad using Lipofectamine 2000 (Thermo Fisher Scientific). The media was changed 4-6 hours after transfection. The cells were split onto coverslips coated with attachment factor protein (Gibco). Electrophysiological recordings were carried out at room temperature 24-48 hours after transfection. The cells were authenticated by ATCC and tested for mycoplasma contamination.

Transgenic mice generation:

The Institutional Animal Care and Use Committee at Columbia University approved all animal experiments. Male and female mixed-strain mice, 6-weeks to 4-months of age were used. Sample sizes exceeded the number of samples determined by power calculations, which were based on effect sizes previously reported [16,17,42,43]. Number of animals was always greater than 3 per genotype. The investigators were blinded to group allocation during data acquisition and analysis.

The transgenic constructs were generated by fusing rabbit α_{1C} cDNA or human β_{2B} cDNA to the modified murine α-myosin heavy chain (MHC) tetracycline-inducible promoter vector (gift of Jeffrey Robbins and Jeffrey Molkentin, University of Cincinnati, Cincinnati, OH) [44,45]. A 3X FLAG-epitope was ligated in-frame to the N-terminus of α_{1C}. The α_{1C} subunit was engineered to be dihydropyridine (DHP)-insensitive with the substitutions T1066Y and Q1070M [46,47]. GFP was ligated to the N-terminus of β_{2B}. The creation of GFP-WT β_{2B} transgenic mice was described previously [17]. The V5 epitope and APEX2 cDNA [5,48], created by gene synthesis, were conjugated to the N-terminus of DHP-resistant-α_{1C} and WT β_{2B}.

The 35-α mutant and the 28-β mutant cDNA were generated by site-directed mutagenesis. The optimal PKA phosphorylation motif is a tetrapeptide with Arg at the 2nd and 3rd positions (termed −2 and −3) prior to the phosphorylated Ser or Thr, and a large hydrophobic residue immediately thereafter (R-R-X-S/T-Φ) [49-51]. The requirement for a positive charge is highest for residues at -2 and -3, but can be found for residues as far as position -6 in PKA target sites [52]. Sites with Arg in positions between −4 and −1 are strongly preferred and to a lesser extent His or Lys [50,53]. We identified all potential intracellular PKA phosphorylation sites (Extended Data Fig. 1a, d) in rabbit α_{1C} and human β_{2B} using both manual sequence analysis and several web-based PKA phosphorylation prediction tools, including pKaPS [54], DISPHOS [55], GPS [56], NETPHOS [57] and SCANSITE [58]. Each phosphorylation site was mutated to Ala. We also mutated additional Ser and Thr within several amino acid residues C-terminal to the Arg or Lys, in order to ensure that we fully captured each phospho-regulatory site. 51 residues in rabbit α_{1C} were replaced with Ala at 35 potential phospho-regulatory domains in the 35-mutant α_{1C} construct, and 37

Author Manuscript Author Manuscript Author Manuscript Author Manuscript

residues were replaced with Ala at 28 putative phospho-regulatory domains of β_{2B}. We excluded those sites predicted to be extracellular or within the plasma membrane.

Transgenic mice with non-targeted insertion of these tetracycline-regulated cDNA (Fig. 1b) were bred with cardiac-specific (α-MHC), doxycycline-regulated, codon-optimized reverse transcriptional trans-activator (rtTA) mice [59] (obtained via the Mutant Mouse Resource and Research Center) to generate double-transgenic mice. For the α_{1C}-APEX2 and β_{2B}-APEX2 mice, transgene expression did not require doxycycline due to a low basal binding of rtTA protein to the *Tet* operator sequences (so-called "leak") [59]. These expression levels result in Ca^{2+} current levels similar to native conditions in heart. The results presented were consistent across all founder lines and gender, and therefore were pooled.

Isolation of adult cardiac myocytes:

Mice ventricular myocytes were isolated by enzymatic digestion using a Langendorff perfusion apparatus as previously described [16,17,42,43,60]. Cardiomyocytes were isolated from 8-12 week-old non-transgenic and transgenic mice.

Proximity labeling biotinylation:

Proximity labeling was performed as described [48] with minor modifications. Isolated ventricular cardiomyocytes were incubated in labeling solution with 0.5 μM biotin-phenol (Iris-biotech) for 30 minutes. For some experiments, during the final 10 minutes of labeling, 1 μM isoproterenol (Sigma I5627) was added. To initiate labeling, H_2O_2 (Sigma H1009) was added to a final concentration of 1 mM for 1 minute. Exactly 1 minute after H_2O_2 treatment, the labeling solution was decanted and cells were washed three times with cold quenching solution containing (in mM) 10 Sodium ascorbate (VWR 95035-692), 5 Trolox (Sigma 238813), and 10 Sodium azide (Sigma S2002). After cells were harvested by centrifugation, the quenching solution was aspirated and the pellet was flash-frozen and stored at −80 °C until streptavidin pull-down.

For biotinylation in Langendorff-perfused hearts, mice were injected with 5 mg/kg Propranolol-HCl (Sigma PHR1308) to suppress adrenergic stimulation during the isoflurane anesthesia and cardiectomy. Hearts were retrograde perfused with Krebs' solution for 10 minutes prior to addition of biotin-phenol for 15 minutes. During the final 5 minutes, 1 μM Isoproterenol (Sigma 1351005) or vehicle was added to the perfusate. Electrocardiograms were monitored throughout the experiment to ensure viability of the preparation and an isoproterenol-induced increase in heart rate.

The cells or whole heart tissue were lysed with a hand-held tip homogenizer in a solution containing (in mM), 50 Tris (tris(hydroxymethyl)aminomethane) , 150 NaCl, 10 EGTA, 10 EDTA, 1% Triton X-100 (v/v), 0.1% SDS (w/v), 10 Sodium ascorbate, 5 Trolox, and 10 Sodium azide, phosphatase inhibitors (Sigma 4906845001), protease inhibitors (Sigma 4693159001), Calpain inhibitor I (Sigma A6185) and Calpain inhibitor II (Sigma A6060). Biotin labeling of the samples was confirmed after size-fractionation of proteins on SDS-PAGE, transfer to nitrocellulose membranes, and probing with Streptavidin-HRP (Thermofisher, S911, Lot# 1711896, 0.6mg/ml). The response to isoproterenol was assessed

Author Manuscript Author Manuscript Author Manuscript Author Manuscript

by immunoblotting with an anti-phospho-phospholamban (Ser16/Thr17) antibody (Cell Signaling, #8496, Lot#1; 1:1000 dilution).

Immunoprecipitation and Immunoblots:

Cardiomyocytes were lysed with a hand-held tip homogenizer in a 1% (v/v) Triton X-100 buffer containing (in mM): 50 Tris-HCl (pH 7.4) 150 NaCl, 10 EDTA, 10 EGTA and protease inhibitors. The lysates were incubated on ice for 30 minutes, centrifuged at 14,000 RPM at 4°C for 10 minutes and supernatants collected. Proteins were size-separated on SDS-PAGE, transferred to nitrocellulose membranes, and probed with anti-V5 antibody (Thermofisher, R960-25; 1:5000 dilution), a custom-made polyclonal anti-α_{1C} antibody (Yenzym, 1:1000 dilution) [61,62], a custom-made polyclonal anti-β antibody (epitope: mouse residues 120-138: DSYTSRPSDSDVSLEEDRE; Yenzym, 1:1000 dilution), an anti-JPH2 antibody (Pierce, PA5-20642, lot# NG1583142; 1:1000 dilution), an anti-calmodulin antibody (Millipore Sigma 05-173; 1:1000 dilution), a custom-made anti-RyR2 antibody (1:5000 dilution) [63], and an anti-$K_V1.5$ antibody (Alomone, APC-150, Lot# APC004AN0850; 1:1000 dilution). Anti-FLAG antibody (Sigma, F7425, Lot#078M4886V) immunoprecipitations were performed, as previously described [17], overnight in a lysis buffer consisting of (in mM): 50 Tris-HCl pH 7.4, 150 NaCl, 0.25% Triton X-100 (v/v), 10 EDTA, 10 EGTA, 0.01 Calpain inhibitor I, 0.01 Calpain inhibitor II, and Complete protease inhibitors (1 per 7 ml, Roche). Antibody-protein complexes were collected using protein A conjugated agarose (Amersham) for 2 h, followed by 3 washes in lysis buffer. Proteins were size-separated by SDS, transferred to nitrocellulose membranes and probed with HRP-conjugated anti-FLAG antibody (Sigma, A8592), a custom-made anti-β antibody and HRP-conjugated secondary goat anti-rabbit antibody. Phospholamban phosphorylation was detected with an anti-phospho-PLB antibody. Detection of luminescence was performed with a CCD camera (Carestream Imaging). The uncut gels are shown in Supplementary Fig. 1.

Immunofluorescence:

Isolated cardiomyocytes were first exposed to biotin-phenol and H_2O_2 as described above. After quenching, the cells were fixed for 15 minutes in 4% paraformaldehyde, washed with glycine/PBS (phosphate-buffered saline) twice, treated with PBST (0.1% Triton X-100 (v/v) in PBS) for 5 minutes, and blocked with 3% BSA (w/v) in PBS for 1 hour. Indirect immunofluorescence was performed using dilutions of 1:500 of anti-V5 antibody (Thermofisher, R960-25) and 1:200 of Alexa594-labeled goat-anti-mouse antibody (Thermofisher, A11032, Lot#2069816), and 1:800 of streptavidin-Alexa Fluor 488 conjugate (Thermofisher, S32354, Lot# 1719656). Images were acquired using a confocal microscopy.

Processing of biotinylated proteins for mass spectrometry:

Proteins were prepared as previously described [7] with some modifications. A detailed protocol of the procedures used was published recently [64]. Proteins were precipitated with Trichloroacetic acid (TCA; Sigma T9159) and then centrifuged at 21,130 × g at 4 °C for 10 minutes. The pellet was washed with −20 °C cold acetone (Sigma 650501), vortexed, and centrifuged at 21,130 × g at 4 °C for 10 minutes. Following centrifugation, acetone was aspirated and the pellet was acetone-washed again three more times. After the last washing

Author Manuscript Author Manuscript Author Manuscript Author Manuscript

step, the pellet was resuspended in: 8M urea, 100 mM sodium phosphate pH 8, 100 mM NH_4HCO_3, and 1% SDS (w/v) and rotated at room temperature until fully dissolved. Re-suspended proteins were centrifuged at 21,130 × g at room temperature for 10 minutes and the cleared supernatant was transferred to a new microcentrifuge tube. To reduce disulfides, 10 mM TCEP-HCl (Thermo Fisher Scientific PG82089) in Milli-Q water titrated to pH 7.5 with NaOH was added. To alkylate free Cys, freshly prepared 400 mM iodoacetamide (Thermo Fisher Scientific 90034) stock solution in 50 mM ammonium bicarbonate was added to the supernatant to a final concentration of 20 mM, immediately vortexed, and incubated in the dark for 25 minutes at room temperature. After alkylation, freshly prepared DTT (dithiothreitol) stock solution was added to 50 mM final concentration to quench alkylation. Water was added to each sample to reach a final concentration of 4 M urea and 0.5% (w/v) of SDS.

A 100 μL suspension equivalent per sample of streptavidin magnetic beads (Thermo Fisher Scientific #88817) was washed twice with 4 M urea, 0.5% SDS (w/v), 100 mM sodium phosphate pH 8 and was added to each sample (about 1 mg), diluting each sample with an equal amount of water to reach a final concentration of 2 M urea, 0.25% SDS (w/v), 50 mM sodium phosphate pH 8 during pulldown. The tubes were rotated overnight at 4 °C. Following streptavidin pull-down, the magnetic beads were washed three times with 4 M urea, 0.5% SDS (w/v), 100 mM sodium phosphate pH 8, and three times with the same buffer without SDS. The beads were transferred to new tubes for the last wash step. Before final pulldown of the beads for mass spectrometry analysis, 5% of beads resuspension was removed for streptavidin-HRP blotting.

On-bead digestion and TMT labeling:

The samples were prepared as previously described [7]. Liquid reagents used were HPLC quality grade. Washed beads were re-suspended in 50 μL of 200mM EPPS (4-(2-Hydroxyethyl)-1-piperazinepropanesulfonic acid) buffer pH 8.5, 2% acetonitrile (v/v) with 1 μL of LysC stock solution (2 mg/ml, Wako), vortexed briefly and incubated at 37°C for 3 hr. Then, 50 μL of trypsin stock (Promega #V5111) diluted 1:100 (v/v) in 200 mM EPPS pH 8.5 was added. After mixing, digests were incubated at 37°C overnight and beads were magnetically removed. Peptides were directly labeled after digest. For this, acetonitrile was added to a concentration of 30% (v/v) and peptides were labeled with TMT 10-plex or 11-plex reagents (Thermo Fisher Scientific #90406 and #A34807) for 1 hr. Reactions were quenched with hydroxylamine at a final concentration of 0.3% (v/v) for 15 minutes and 1% of labeled peptides were analyzed for efficiency of label incorporation and relative ratios by mass spectrometry. After quenching, peptide solutions were acidified with formic acid, trifluoroacetic acid (TFA) was added to a concentration of 0.1% and peptides were desalted and fractionated by high pH reversed phase chromatography (Thermo Fisher Scientific #84868). After loading of labeled peptides onto pre-conditioned columns and a single wash with water, excess unincorporated TMT label was removed by washing reversed phase columns once with 0.1% trimethylamine (TEA) buffer containing 5% acetonitrile. Samples were fractionated under alkaline conditions into 12 fractions with increasing concentrations of acetonitrile: 10%, 12.5%, 15%, 17.5%, 20%, 25%, 30%, 35%, 40%, 50%, 65% and 80%. Fractions 1 and 7, 2 and 8, 3 and 9, 4 and 10, 5 and 11, 6 and 12 were pooled to obtain 6

Author Manuscript Author Manuscript Author Manuscript Author Manuscript

final pooled fractions for subsequent analysis. Pooled fractions were dried to completion and further purified and desalted by acidic C_{18} solid phase extraction (StageTip). Labeled peptides were finally re-suspended in 1% formic acid (v/v) and 3% acetonitrile (v/v).

Whole cell proteomics: Cell lysis, protein digest and TMT labeling mass spectrometry analysis:

Cells were lysed by homogenization (QIAshredder cartriges, Qiagen) in lysis buffer (2% SDS, 150 mM NaCl, 50 mM Tris pH 7.4). Lysates were reduced with 5 mM DTT, alkylated with 15 mM iodoacetamide for 30 minutes in the dark, alkylation reactions quenched with freshly prepared DTT added to a concentration of 50 mM and proteins precipitated by methanol/chloroform precipitation. Digests were carried out in 1M urea freshly prepared in 200 mM EPPS pH 8.5 in presence of 2% acetonitrile (v/v) with LysC (Wako, 2 mg/ml, used 1:75 w/w protease:substrates during digest) for 3 hours at room temperature and after subsequent addition of trypsin (Promega #V5111, stock 1:100 w/w protease:substrates) over night at 37°C. Missed cleavage rate was assayed from a small aliquot by mass spectrometry. For whole proteome analysis, digests containing approximately 60 µg of peptide material were directly labeled with TMT reagents (Thermo Fisher Scientific). Labeling efficiency and TMT ratios were assayed by mass spectrometry, while labeling reactions were stored at −80°C. After quenching of TMT labeling reactions with hydroxylamine, TMT labeling reactions were mixed, solvent evaporated to near completion and TMT labeled peptides purified and desalted by acidic reversed phase C_{18} chromatography. Peptides were then fractionated by alkaline reversed phase chromatography into 96 fractions and combined into 24 samples.

Mass spectrometry analysis:

Data collection followed a MultiNotch MS^3 TMT method [65] using an Orbitrap Lumos mass spectrometer coupled to a Proxeon EASY-nLC 1200 liquid chromatography (LC) system (both Thermo Fisher Scientific). The capillary column used was packed with C_{18} resin (35 cm length, 75 µm inner diameter, matrix 2.6 µm Accucore (Thermo Fisher Scientific)). Peptides of each fraction were separated for 4 hours over acidic acetonitrile gradients by LC prior to mass spectrometry (MS) analysis. The scan sequence started with an MS^1 scan (Orbitrap analysis; resolution 120,000; mass range 400–1400 Th). MS^2 analysis followed collision-induced dissociation (CID, CE=35) with a maximum ion injection time of 150-300 ms and an isolation window of 0.4 m/z. In order to obtain quantitative information, MS^3 precursors were fragmented by high-energy collision-induced dissociation (HCD) and analyzed in the Orbitrap at a resolution of 50,000 at 200 Th. Further details on LC and MS parameters and settings used were described recently [66].

Peptides were searched with a SEQUEST (v.28, rev. 12) based software against a size-sorted forward and reverse database of the *M. musculus* proteome (Uniprot 07/2014) with added common contaminant proteins. For this, spectra were first converted to mzXML. Searches were performed using a mass tolerance of 20 ppm for precursors and a fragment ion tolerance of 0.9 Da. For the searches maximally 2 missed cleavages per peptide were allowed. We searched dynamically for oxidized methionine residues (+15.9949 Da) and where indicated for phospho-modification of S,T and Y residues (+79.9663 Da). We applied

Author Manuscript Author Manuscript Author Manuscript Author Manuscript

a target decoy database strategy and a false discovery rate (FDR) of 1% was set for peptide-spectrum matches following filtering by linear discriminant analysis (LDA) [26,66]. The FDR for final collapsed proteins was 1%. MS^1 data were calibrated post search and searches performed again. A modified version of the Ascore algorithm was used to quantify the confidence assignment of phosphorylation sites. Phosphorylation localized to particular residues required Ascore values > 13 ($p \leq 0.05$) for confident localization [26]. Quantitative information on peptides was derived from MS^3 scans. Quant tables were generated requiring an MS^2 isolation specificity of >70% for each peptide and a sum of TMT signal to noise (s/n) of >200 over all channels for any given peptide and exported to Excel and further processed therein. Details of the TMT intensity quantification method and further search parameters applied were described previously previously [67]. Proteomics raw data and search results were deposited in the PRIDE archive [68,69] and can be accessed under ProteomeXchange accession nunbers: PXD014499, PXD014500, PXD014501.

The relative summed TMT s/n for proteins between two experimental conditions (referred to as “enrichment” in the text) was calculated from the sum of TMT s/n for all peptides quantified of a given protein. For gene ontology (GO) term enrichment, the BINGO package in Cytoscape was used [70]. Scaled quantification data were subjected to two-way clustering (JMP software package) and changes in enrichment were analyzed using Graphpad Prism 8 (Graphpad Software). Statistical significance was determined by multiple t-tests without correction for multiple comparisons and α=0.05. Data for relative protein quantification accompany this paper in the form of Supplementary Data Tables 1,3-6, and can be accessed online.

Purification of GFP-conjugated Rad and phosphoproteomic analysis:

HEK293T cells were cultured in DMEM with 10% FBS and 1% Pen-Strep. Cells were transfected with GFP-Rad using lipofectamine 2000 as described above. Media was changed 4-6 hours after transfection. After 24 hours, cells were treated with trypsin and spun down for 5 minutes at 1000 rpm. Cells were then resuspended in PBS with 10 μM forskolin for 5 minutes. After washing cell pellets three times with phosphate-buffered saline (PBS), cells were frozen at −80°C. Cold cell pellets were lysed in PBS with 0.1% triton X-100 (v/v, Sigma) and a phosphatase inhibitor mixture (PhosSTOP, Roche) by pipetting up and down several times. Lysates were homogenized by passing them through QIAshredder cartridges (Qiagen) and incubated with GFP-trap agarose beads (Chromotek, Germany) for 4 hours at 4°C with constant rotation. Beads were washed 3 times with PBS with 0.1% (v/v) Triton and three times with detergent-free PBS and subjected to on-bead digest with trypsin (Promega #V5111), LysC (Wako) or ArgC (Promega #V1881, ArgC digestion buffer 50 mM Tris-HCL pH 7.8, 5 mM $CaCl_2$, 2 mM EDTA, 2% acetonitrile (v/v)) separately as described above overnight at 37°C. After acidification, peptides were purified by reversed phase C_{18} chromatography and subjected to MS/MS analysis. For this, the same parameters as above for MS^1 and MS^2 scans were used with an isolation window of 1.2 Da and taking neutral loss of 97.9763 Da into account with multi-stage activation (MSA) set for MS^2 scans. Analysis of phospho-site localization was performed as described above.

Author Manuscript Author Manuscript Author Manuscript Author Manuscript

Fractional shortening:

Freshly isolated myocytes were perfused with a Tyrode's solution containing 1.8 mM $CaCl_2$. Myocytes were field stimulated at 1-Hz. Nisoldipine (300 nM) dissolved in Tyrode's solution was then superfused. Fractional shortening of sarcomere length was measured using the SarcLen module of Ionoptix.

Whole cell patch clamp electrophysiology:

Isolated cardiomyocytes or HEK cells on glass 8×8 mm coverslips were placed in Bioptechs Delta T Dishes filled with solution containing (in mM): 112 NaCl, 5.4 KCl, 1.7 NaH_2PO4. 1.6 $MgCl_2$, 20.4 HEPES (pH 7.2), 30 Taurine, 2 DL-Carnitine, 10.3 Creatine, 5.4 Glucose. The petri dishes were mounted on the stage of an inverted microscope and served as a perfusion chamber. After establishing a seal and achieving whole-cell configuration, external solutions were changed by fast local perfusion method.

For cardiomyocytes, pipette resistance was between 1-3 MΩ. Membrane currents were measured by conventional (ruptured) whole-cell patch-clamp method using a MultiClamp 700B or Axopath200B amplifier and pCLAMP 10.7 software (Molecular Devices). Capacitance transients and series resistance were compensated. Voltage was corrected for liquid junction potential (−10 mV) during analysis. Leak currents were subtracted by a P/4 protocol. The parameters of voltage-dependent activation were obtained using a modified Boltzmann distribution: $I(V)= G_{max} * (V-E_{rev})/[1 + \exp(V-V_{50})/V_c)]$, where I(V) is peak current, G_{max} is maximal conductance, E_{rev} is reversal potential, V_{50} is the midpoint, and V_c is the slope factor.

The pipette solution contained (in mM): 40 CsCI, 80 Cesium Gluconate, 10 BAPTA (1,2-bis(*o*-aminophenoxy)ethane- *N*,*N*,*N*′, N′-tetraacetic acid), 1 $MgCl_2$, 4 Mg-ATP, 2 $CaCl_2$, and 10 HEPES (4-(2-hydroxyethyl)-1-piperazineethanesulfonic acid), adjusted to pH 7.2 with CsOH. After the isolated cardiomyocytes were dialyzed and adequately buffered with 10 mM BAPTA in the internal solution, cells were superfused with (in mM): 140 TEA-Cl (Tetraethylammonium chloride), 1.8 $CaCl_2$, 1 $MgCl_2$, 10 glucose, and 10 HEPES, adjusted to pH 7.4 with CsOH. To measure peak currents, the cell membrane potential was held at −50 mV and stepped to +0 mV for 350 ms every 10 s. To evaluate the current-voltage (I-V) relationship in cardiomyocytes, the same protocol was repeated with steps between −40 mV to +60 mV in 10 mV increments. Nisoldipine (Santa Cruz) was stored protected from light at −20 °C as 3 mM stock in ethanol. The final dilution of nisoldipine to 300 nM was in the extracellular recording solution immediately prior to the experiment. Isoproterenol (Sigma I5627) and Forskolin (Santa Cruz) were prepared daily and diluted in extracellular solution.

For HEK293T cell experiments involving the Forskolin-induced stimulation of $Ca_V1.2$, $Ca_V1.3$ and $Ca_V2.2$ currents, perforated whole-cell patch clamp technique was implemented to minimize current run-down and preserve the intracellular milieu. Amphotericin B (Sigma A9528) was initially dissolved in DMSO (20 mg/ml) and used in the pipette solution at a final concentration of 200 μg/ml. The tip of pipette was filled with amphotericin-free solution (in mM): 80 Cesium Gluconate, 40 CsCI, 10 HEPES, 10 BAPTA, 1 $MgCI_2$, 1 Mg-ATP, pH adjusted to 7.2 with CsOH. The pipette was backfilled with (in mM): 125 CsCI, 10

Author Manuscript Author Manuscript Author Manuscript Author Manuscript

HEPES, 4 $CaCI_2$, 1 $MgCI_2$, pH-7.2 with CsOH; containing amphotericin, 200 μg/ml. $CaCI_2$ (4 mM) was added to the patch electrode solution to enable the detection of conversion from perforated to ruptured configuration. The external solution contained (in mM): 130 tetraethylammonium methanesulfonate, 10 HEPES, 1 $MgCI_2$,10 (with Rad expression) or 2 (without Rad expression) $BaCI_2$, 5 Glucose. For experiments with HEK293T cells, in addition to step protocols, we used a ramp protocol with a 200-ms voltage ramp from −60 to +60 mV (0.6 V/s) applied every 10-seconds to monitor the I-V relationship. All experiments were performed at room temperature, 22 ± 1° C. Cells were selected based on co-transfection of a vector containing GFP in the absence of Rad, and GFP-conjugated Rad for the experiments with Rad transfected. For both cardiomyocytes and HEK293T cells, cells without a stable baseline (potentially due to run-down or run-up) were not studied.

Voltage steps protocol used in cardiomyocytes studies evaluated $I_{Ipeak} = I_{peak}$ (V), which was recalculated in CLAMPFIT to G=G(V) as $G=I/(V-E_{rev})$. For HEK cells experiments, we used a ramp protocol (Extended Data Fig. 8b). The experimental records were I=I(t), where t=time. We transformed these records to I=I(V), which was then further transformed to G=G(V) in CLAMPFIT (see Extended Data Fig. 8b). The parameters of voltage-dependent activation were obtained using a modified Boltzmann distribution. A nonlinear fit with Boltzmann sigmoidal function was done in Prism (GraphPad) with goodness of fit: $R^2>0.99$.

Single channel patch clamp electrophysiology:

Cell-attached single-channel recordings were performed at room temperature as previously described [71,72]. Patch pipettes (5–10 MΩ) were pulled from ultra-thick-walled borosilicate glass (BF200-116-10, Sutter Instruments), and coated with Sylgard. Currents were filtered at 2 kHz. The pipette solution contained (in mM): 140 tetraethylammonium methanesulfonate; 10 HEPES; 40 $BaCl_2$; at 300 mOsm/L, adjusted with tetraethylammonium methanesulfonate; and pH 7.4 adjusted with tetraethylammonium hydroxide. To maintain the membrane potential at 0 mV, the bath contained (in mM): 132 potassium glutamate; 5 KCl; 5 NaCl; 3 $MgCl_2$; 2 EGTA (ethylene glycol-bis(β-aminoethyl ether)-N,N,N′,N′-tetraacetic acid); 10 glucose; 20 HEPES; at 300 mOsm/L adjusted with glucose; and pH 7.4 adjusted with NaOH. Cell-attached single-channel currents were measured during 200 ms voltage ramps between −80 to +70 mV (portions between −50 and 40 mV displayed and analyzed). For each patch, we recorded 80-120 sweeps with a repetition interval of 10 seconds.

The sample size for the P_o-V relationships:

α_{1C}	n = 10 (3 transfections)	933 sweeps
α_{1C} +PKA	n = 5 (2 transfections)	450 sweeps
Rad	n = 5 (3 transfections)	372 sweeps
Rad+PKA	n = 8 (3 transfections)	527 sweeps
Rad Mut	n = 6 (4 transfections)	388 sweeps
Rad Mut+PKA	n = 5 (3 transfections)	439 sweeps

Author Manuscript Author Manuscript Author Manuscript Author Manuscript

The modal analysis are histograms of single-trial average P_o values obtained from one-channel patches. For P_o-V analysis, we conservatively corrected for shifts in voltage. The number of sweeps is as follows:

α_{1C} alone:	281 sweeps (from 3 one-channel patches)
Rad:	372 sweeps (from 5 one-channel patches)
Rad + PKA:	311 sweeps (from 3 one-channel patches)

Flow Cytometric FRET 2-hybrid assay:

For flow cytometric FRET assay, HEK293 cells (ATCC CRL1573) were cultured in 12 well plates and transfected with polyethylenimine (PEI) 25 kDa linear polymer (Polysciences #2396602). Briefly, 1.5 μg of Cerulean (Cer) and Venus (Ven) -tagged cDNA pairs were mixed together in 100 μl of serum-free DMEM media and 6 μl of PEI is added to each sterile tube. FRET experiments were performed 1-day post-transfection. Protein synthesis inhibitor cycloheximide (100 μM) was added to cells 2-hrs prior to experimentation to halt synthesis of new fluorophores to allow existing fluorophores to fully mature.

For FRET measurements, we utilized an LSR II (BD Biosciences) flow cytometer equipped with 405 nm, 488 nm, and 633 nm lasers for excitation and 18 different emission channels. Forward and side scatter signals were detected and used to gate for single, and healthy cells. For determining FRET efficiency, we measured three distinct fluorescence signals: (1) S_{Cer} corresponding to cerulean emission is measured through the BV421 channel (excitation, 405 nm; emission, 450/50), (2) S_{Ven} corresponding to venus emission measured via FITC channel (excitation, 405 nm; dichroic, 505LP; emission, 525/50), and (3) S_{FRET} corresponding to FRET emission via the BV510 channel (excitation, 405 nm; dichroic, 505LP; emission, 525/50). These raw fluorescence measurements are subsequently used to obtain $\mathrm{Ven}_{\mathrm{direct}}$ (venus emission due to direct excitation), $\mathrm{Cer}_{\mathrm{direct}}$ (cerulean emission due to direct excitation), and $\mathrm{Ven}_{\mathrm{FRET}}$ (venus emission due to FRET excitation). Flow cytometric signals were collected at medium flow rate (2k-8k events/sec). Fluorescence data was exported as FCS 3.0 files for further processing and analysis using custom MATLAB functions (MathWorks).

For each experimental run on the flow cytometer, we performed several control experiments: (1) Background fluorescence level for each fluorescent channel (BG_{Cer}, BG_{Ven}, and BG_{FRET}) was obtained by measuring fluorescence from cells exposed to PEI without any fluorophore containing plasmids. (2) Cells expressing Ven fluorophore alone were utilized to measure spectral crosstalk parameter R_{A1}, corresponding to bleed-through of Ven fluorescence into the FRET channel. (3) Cells expressing cerulean fluorophore alone were used to measure spectral crosstalk parameter R_{D1} and R_{D2}, corresponding to bleed-through of cerulean fluorescence into FRET and Ven channels respectively. (4) FRET measurements also require determination of instrument-specific calibration parameters g_{Ven} / g_{Cer} and f_{Ven} / f_{Cer}, corresponding to ratios of fluorescence excitation and emission for Ven to cerulean fluorophores. These parameters also incorporate fluorophore-dependent aspects including molar extinction (for g) and quantum yield (for f) as well as instrument specific parameters

Author Manuscript Author Manuscript Author Manuscript Author Manuscript

including laser power, attenuation by optical components, as well as photodetection, amplification, and digitization of fluorescence. For determination of these parameters, we utilized Cer-Ven dimers with four different linker lengths (5, 32, 40, and 228). (5) Co-expression of cerulean and Ven fluorophores provided estimates for concentration-dependent collisional FRET.

For our experiments, $R_{A1} \sim 0.11$, $R_{D1} \sim 2.8$, and $R_{D2} \sim 0.006$. We observed only minor day-to-day variation in these measurements. For each cell, spectral cross-talk was subtracted as follows:

$$Cer_{\text{direct}} = R_{D1} \cdot S_{\text{Cer}},\ Ven_{\text{direct}} = R_{A1} \cdot (S_{\text{Ven}} - R_{D2} \cdot S_{\text{Cer}},\ \text{and}\ Ven_{\text{FRET}} = S_{\text{FRET}} - R_{A1} \cdot (S_{\text{Ven}} - R_{D2} \cdot S_{\text{Cer}}) - R_{D1} \cdot S_{\text{Cer}}.$$

Following spectral unmixing, we obtained $g_{\text{Ven}} / g_{\text{Cer}}$ and $f_{\text{Ven}} / f_{\text{Cer}}$ from data for Cer-Ven dimers by determining the slope and intercept for the following linear relationship:

$$\frac{Ven_{FRET}}{Cer_{\text{direct}}} = \frac{g_{\text{Cer}}}{g_{Ven}} \bullet \frac{Ven_{direct}}{Cer_{\text{direct}}} - \frac{f_{Ven}}{f_{Cer}}$$

For typical experiments, $g_{\text{Ven}} / g_{\text{Cer}} = 0.0194$ and $f_{\text{Ven}} / f_{\text{Cer}} = 2.3441$. Having obtained these calibration values, donor-centric FRET efficiencies were computed as,

$$E_D = \frac{Ven_{\text{FRET}}}{Ven_{\text{FRET}} + \frac{f_{Ven}}{f_{Cer}} \bullet Cer_{\text{direct}}}$$

For Cer-Ven dimers, FRET efficiencies of ~ 0.55, 0.38, and 0.05 were obtained for linker lengths 5, 32, and 228 respectively, matching previous work [30]. The relative proportion of Cerulean and Venus fluorophores in each cell was determined as $N_{\text{Cer}} = \text{Cer}_{\text{direct}} / (1 - E_D)$ and $N_{\text{Ven}} = \text{Ven}_{\text{direct}} / (g_{\text{Ven}} / g_{\text{Cer}} \times f_{\text{Ven}} / f_{\text{Cer}})$. To construct FRET 2-hybrid binding curves, we imposed a 1:1 binding isotherm as in previous studies [30]. For each FRET pairs, $K_{d,\text{EFF}}$ and $E_{D,\text{max}}$ and 95% - confidence intervals were obtained by constrained least squares fit.

For Fig. 4b-c and Extended Data Fig. 9a-b, we show all the individual cells from two different transfections. We fit these data with the equation: $E_D = E_{max}*[\text{Ven-Rad}]_{free}/([\text{Ven-Rad}]_{free} + \text{kdeff})$ using least squares algorithm (https://www.mathworks.com/help/stats/nlinfit.html). The Kdeff fit value based on all the data points is shown as the bar in Extended Data Fig. 9c. The error is calculated by the fitting algorithm as a 95%-confidence interval on the fit parameter: https://www.mathworks.com/help/stats/nlparci.html).

Statistical Analysis:

Results are presented as mean ± SEM. For comparisons between two groups, Student's t-test was used. Statistical analyses were performed using Prism 8 (Graphpad Software). For multiple group comparisons, a one-way ANOVA followed by either Dunnett's or Tukey's

Author Manuscript Author Manuscript Author Manuscript Author Manuscript

post-hoc test were performed using Prism 8. Differences were considered statistically significant at values of $P < 0.05$.

Extended Data

Author Manuscript Author Manuscript Author Manuscript Author Manuscript

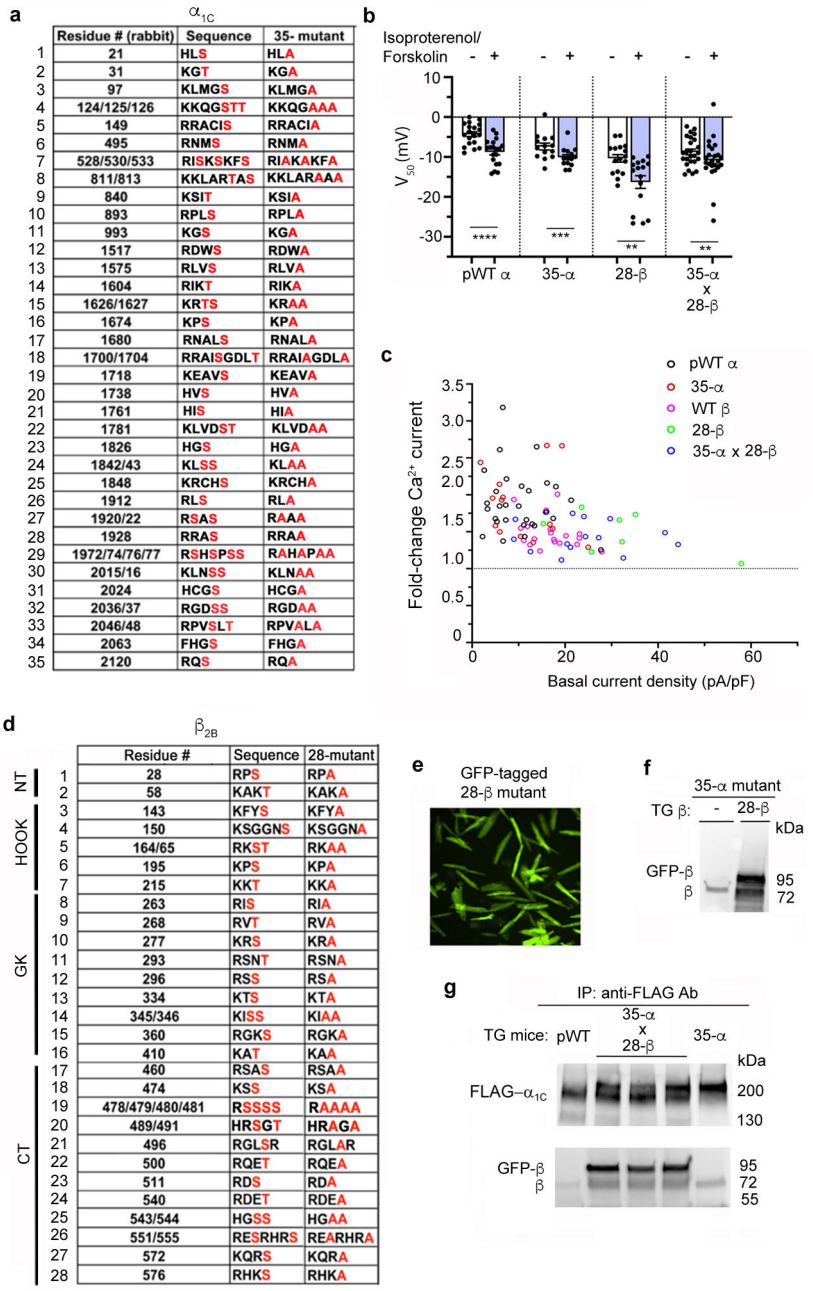

	Residue # (rabbit)	Sequence	35- mutant
1	21	HLS	HLA
2	31	KGT	KGA
3	97	KLMGS	KLMGA
4	124/125/126	KKQGSTT	KKQGAAA
5	149	RRACIS	RRACIA
6	495	RNMS	RNMA
7	528/530/533	RISKSKFS	RIAKAKFA
8	811/813	KKLARTAS	KKLARAAA
9	840	KSIT	KSIA
10	893	RPLS	RPLA
11	993	KGS	KGA
12	1517	RDWS	RDWA
13	1575	RLVS	RLVA
14	1604	RIKT	RIKA
15	1626/1627	KRTS	KRAA
16	1674	KPS	KPA
17	1680	RNALS	RNALA
18	1700/1704	RRAISGDLT	RRAIAGDLA
19	1718	KEAVS	KEAVA
20	1738	HVS	HVA
21	1761	HIS	HIA
22	1781	KLVDST	KLVDAA
23	1826	HGS	HGA
24	1842/43	KLSS	KLAA
25	1848	KRCHS	KRCHA
26	1912	RLS	RLA
27	1920/22	RSAS	RAAA
28	1928	RRAS	RRAA
29	1972/74/76/77	RSHSPSS	RAHAPAA
30	2015/16	KLNSS	KLNAA
31	2024	HCGS	HCGA
32	2036/37	RGDSS	RGDAA
33	2046/48	RPVSLT	RPVALA
34	2063	FHGS	FHGA
35	2120	RQS	RQA

		Residue #	Sequence	28-mutant
NT	1	28	RPS	RPA
	2	58	KAKT	KAKA
HOOK	3	143	KFYS	KFYA
	4	150	KSGGNS	KSGGNA
	5	164/65	RKST	RKAA
	6	195	KPS	KPA
	7	215	KKT	KKA
GK	8	263	RIS	RIA
	9	268	RVT	RVA
	10	277	KRS	KRA
	11	293	RSNT	RSNA
	12	296	RSS	RSA
	13	334	KTS	KTA
	14	345/346	KISS	KIAA
	15	360	RGKS	RGKA
	16	410	KAT	KAA
CT	17	460	RSAS	RSAA
	18	474	KSS	KSA
	19	478/479/480/481	RSSSS	RAAAA
	20	489/491	HRSGT	HRAGA
	21	496	RGLSR	RGLAR
	22	500	RQET	RQEA
	23	511	RDS	RDA
	24	540	RDET	RDEA
	25	543/544	HGSS	HGAA
	26	551/555	RESRHRS	REARHRA
	27	572	KQRS	KQRA
	28	576	RHKS	RHKA

Extended Data Fig. 1. Putative PKA phosphorylation sites in α_{1C} and β_{2B} subunit.

(a) The 35 putative PKA phosphorylation sites in rabbit α_{1C}. The 51 residues in red are either predicted phosphorylation sites or within the immediate region of the predicted phosphorylation sites. All 51 residues were replaced with Ala in the 35-mutant α_{1C} transgenic mice. **(b)** Combined bar and column scatter plot of Boltzmann function parameters V_{50}. Mean ± SEM. ** P<0.01; *** P<0.001; **** P<0.0001 by paired two-tailed t-test. pWT α, n= 19; 35-α mutant, n= 14; 28-β mutant, n= 16; 35-α mutant X 28-β mutant, n= 24. Specific P values can be found in the Source Data associated with this figure. **(c)** Graph of isoproterenol and forskolin-induced increase in nisoldipine-resistant current stratified by total basal current density before nisoldipine. **(d)** The 28 putative PKA

Author Manuscript Author Manuscript Author Manuscript Author Manuscript

phosphorylation sites in the N-terminal (NT), Hook, GK and C-terminal (CT) domains of β_{2B}. The 37 residues in red are either predicted phosphorylation sites or within the immediate vicinity of predicted phosphorylation sites, and were mutated to Ala in the 28-mutant GFP-tagged β_{2B} transgenic mice. **(e)** Fluorescence imaging of isolated cardiomyocytes expressing GFP-tagged 28-β mutant. Representative of images from more than 5 biologically independent mice. **(f)** Anti-β antibody immunoblot of cleared lysates from doxycycline-fed 35-mutant α_{1C} transgenic mice or 35-mutant α_{1C} X GFP-tagged 28-mutant β_{2B} expressing mice hearts. Representative of immunoblots obtained from at least 3 biologically independent mice. **(g)** Anti-FLAG antibody (upper) and anti-β antibody (lower) immunoblots of anti-FLAG antibody immunoprecipitations from cleared lysates of hearts from pWT, 35-α and three 35-α X GFP-tagged-28-β expressing mice. Representative images of two independent experiments. For source gel data, see Supplementary Fig. 1.

Author Manuscript Author Manuscript Author Manuscript Author Manuscript

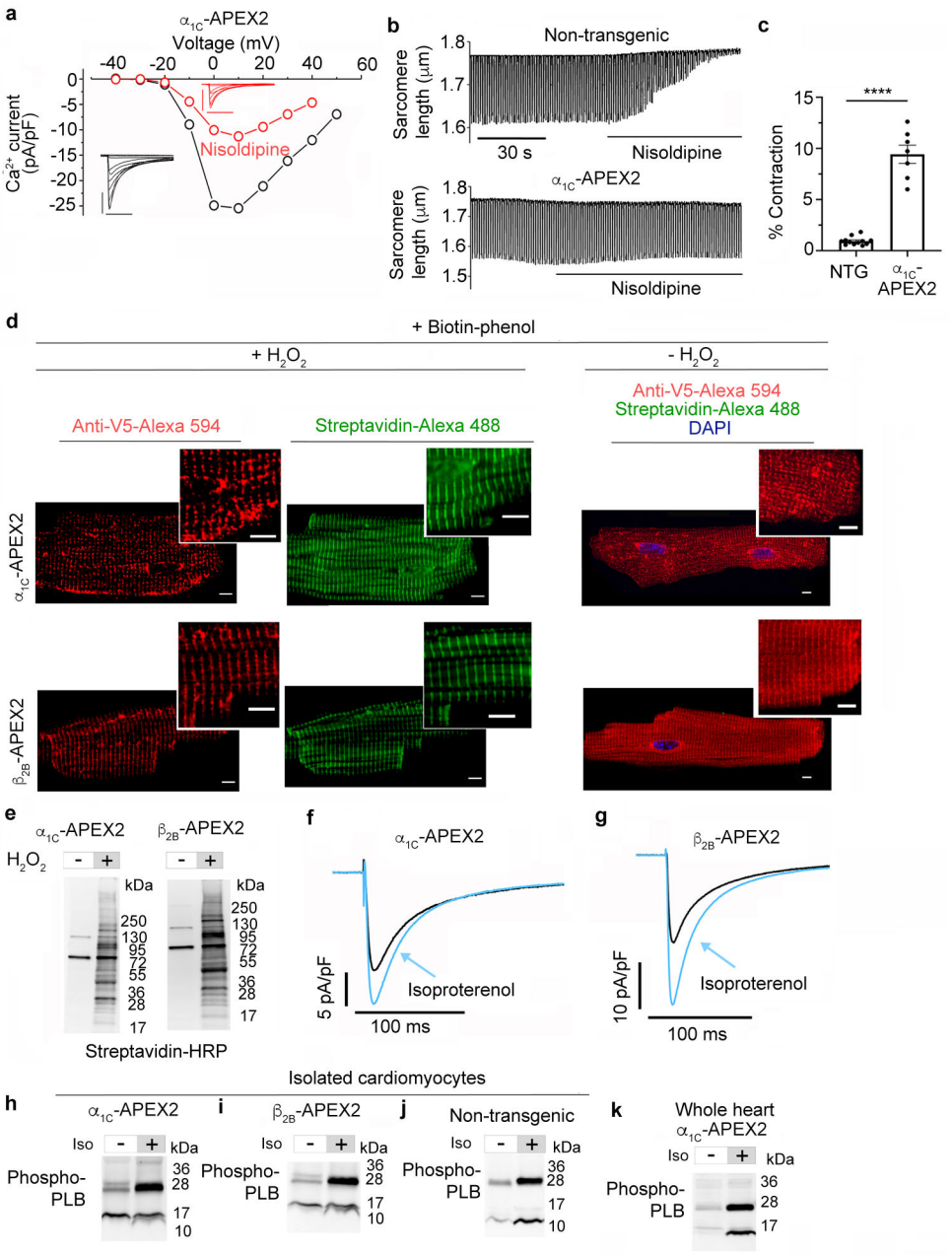

Extended Data Fig. 2. Trafficking and function of APEX2-conjugated $Ca_V1.2$ channels subunits in heart.

(a) Exemplar current-voltage relationship of Ca^{2+} currents from α_{1C}-APEX2 mice cardiomyocytes acquired in absence (black trace) and presence of nisoldipine (red trace). Inset scale bars: horizontal 100 ms, vertical 10 pA/pF. Representative of 5 experiments. **(b)** Time course of changes in sarcomere length after superfusion of nisoldipine-containing solution. Representative of 7 experiments **(c)** Percent-shortening in the presence of nisoldipine. Mean ± SEM. ****, P<0.0001 by unpaired two-tailed t-test. n=12, 7 cardiomyocytes, respectively. **(d)** Immunofluorescence of cardiomyocytes isolated from α_{1C}-APEX2 and β_{2B}-APEX2 expressing mice exposed to biotin-phenol and H_2O_2 or no

Author Manuscript Author Manuscript Author Manuscript Author Manuscript

H_2O_2. Nuclear labeling with DAPI stain. Scale bar = 5 μm. Representative of 5 and 8 cardiomyocytes from 2 and 3 mice respectively. **(e)** Streptavidin-horseradish peroxidase (HRP) blot of lysates of isolated ventricular cardiomyocytes. Blot representative of 5 similar experiments. **(f)** Exemplar whole-cell $Ca_V1.2$ currents recorded from cardiomyocytes of α_{1C}-APEX2 transgenic mice. Black trace: 300 nM nisoldipine; blue trace: 200 nM isoproterenol + nisoldipine. Representative of 9 cells from 2 biologically independent mice. **(g)** Same as (f) except from β_{2B}-APEX2 transgenic mice. Black trace: control; blue trace: 200 nM isoproterenol. Representative of 7 experiments from 2 biologically independent mice. **(h-j)** Anti-phospho-phospholamban antibody immunoblot of isolated cardiomyocytes exposed to 1 μM isoproterenol. For cardiomyocytes isolated from α_{1C}-APEX2 and β_{2B}-APEX2 mice, the cardiomyocytes were exposed to isoproterenol after incubation with biotin-phenol. Blots representative of 3 independent experiments from at least 5 biologically independent mice for each genotype. **(k)** Same as (h-j) except whole heart exposed to 1 μM isoproterenol for 5 minutes after infusion of biotin-phenol. Blots representative of at least 5 biologically independent mice for no isoproterenol and at least 5 biologically independent mice for isoproterenol. For source gel data, see Supplementary Fig. 1.

Author Manuscript Author Manuscript Author Manuscript Author Manuscript

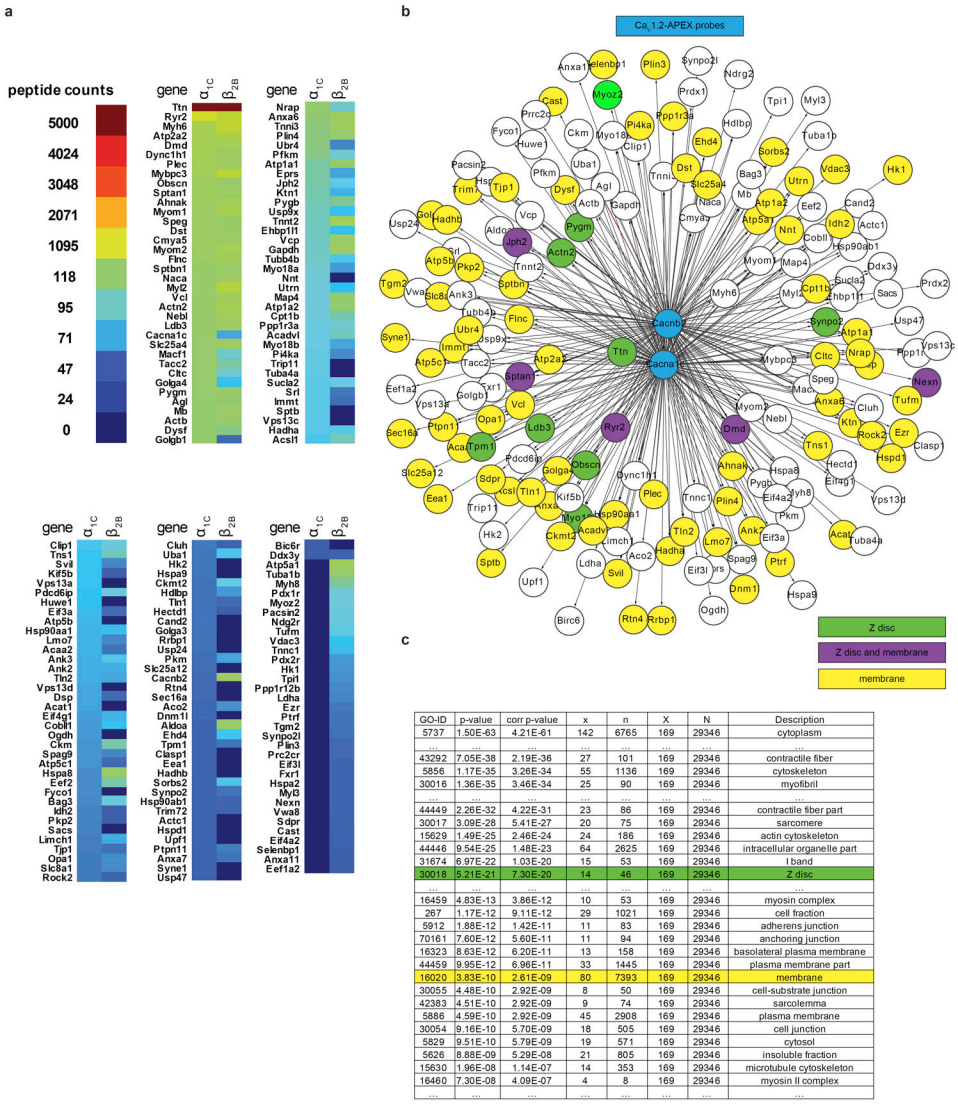

GO-ID	p-value	corr p-value	x	n	X	N	Description
5737	1.50E-63	4.21E-61	142	6765	169	29346	cytoplasm
...	...	...	...	...	...	...	...
43292	7.05E-38	2.19E-36	27	101	169	29346	contractile fiber
5856	1.17E-35	3.26E-34	55	1136	169	29346	cytoskeleton
30016	1.36E-35	3.46E-34	25	90	169	29346	myofibril
...	...	...	...	...	...	...	...
44449	2.26E-32	4.22E-31	23	86	169	29346	contractile fiber part
30017	3.09E-28	5.41E-27	20	75	169	29346	sarcomere
15629	1.49E-25	2.46E-24	24	186	169	29346	actin cytoskeleton
44446	9.54E-25	1.48E-23	64	2625	169	29346	intracellular organelle part
31674	6.97E-22	1.03E-20	15	53	169	29346	I band
30018	5.21E-21	7.30E-20	14	46	169	29346	Z disc
...	...	...	...	...	...	...	...
16459	4.83E-13	3.86E-12	10	53	169	29346	myosin complex
267	1.17E-12	9.11E-12	29	1021	169	29346	cell fraction
5912	1.88E-12	1.42E-11	11	83	169	29346	adherens junction
70161	7.60E-12	5.60E-11	11	94	169	29346	anchoring junction
16323	8.63E-12	6.20E-11	13	158	169	29346	basolateral plasma membrane
44459	9.95E-12	6.96E-11	33	1445	169	29346	plasma membrane part
16020	3.83E-10	2.61E-09	80	7393	169	29346	membrane
30055	4.48E-10	2.92E-09	8	50	169	29346	cell-substrate junction
42383	4.51E-10	2.92E-09	9	74	169	29346	sarcolemma
5886	4.59E-10	2.92E-09	45	2908	169	29346	plasma membrane
30054	9.16E-10	5.70E-09	18	505	169	29346	cell junction
5829	9.51E-10	5.79E-09	19	571	169	29346	cytosol
5626	8.88E-09	5.29E-08	21	805	169	29346	insoluble fraction
15630	1.96E-08	1.14E-07	14	353	169	29346	microtubule cytoskeleton
16460	7.30E-08	4.09E-07	4	8	169	29346	myosin II complex
...	...	...	...	...	...	...	...

Extended Data Fig. 3. Analysis of proteins quantified by mass spectrometry in cardiomyocytes isolated from α_{1C}-APEX2 and β_{2B}-APEX2 mice.

(a) Proteins with a ratio of >2 (measured by normalized TMT signal/noise) in the experimental conditions compared to a no-labeling control (no H_2O_2) are sorted by spectral counts. The 150 proteins with the highest peptide counts are displayed in the color-coded table. α_{1C}-APEX2 and β_{2B}-APEX2 data were collected in biological duplicate experiments. The full table with 3883 proteins quantified by multiplexed SPS MS^3 TMT mass spectrometry is reported in Supplementary Data Table 1. **(b)** Prefuse force directed map of proteins from (a). Peptide counts were used as weight. Proteins mapping to the GO-terms "Z disc" are colored in green, to "membrane" in yellow and to both in purple. The α_{1C}-APEX2 and β_{2B}-APEX2 are colored in blue. **(c)** Gene-ontology (GO) term (cellular localization) enrichment for proteins in (a). The full table is reported in Supplementary Data Table 2.

Author Manuscript Author Manuscript Author Manuscript Author Manuscript

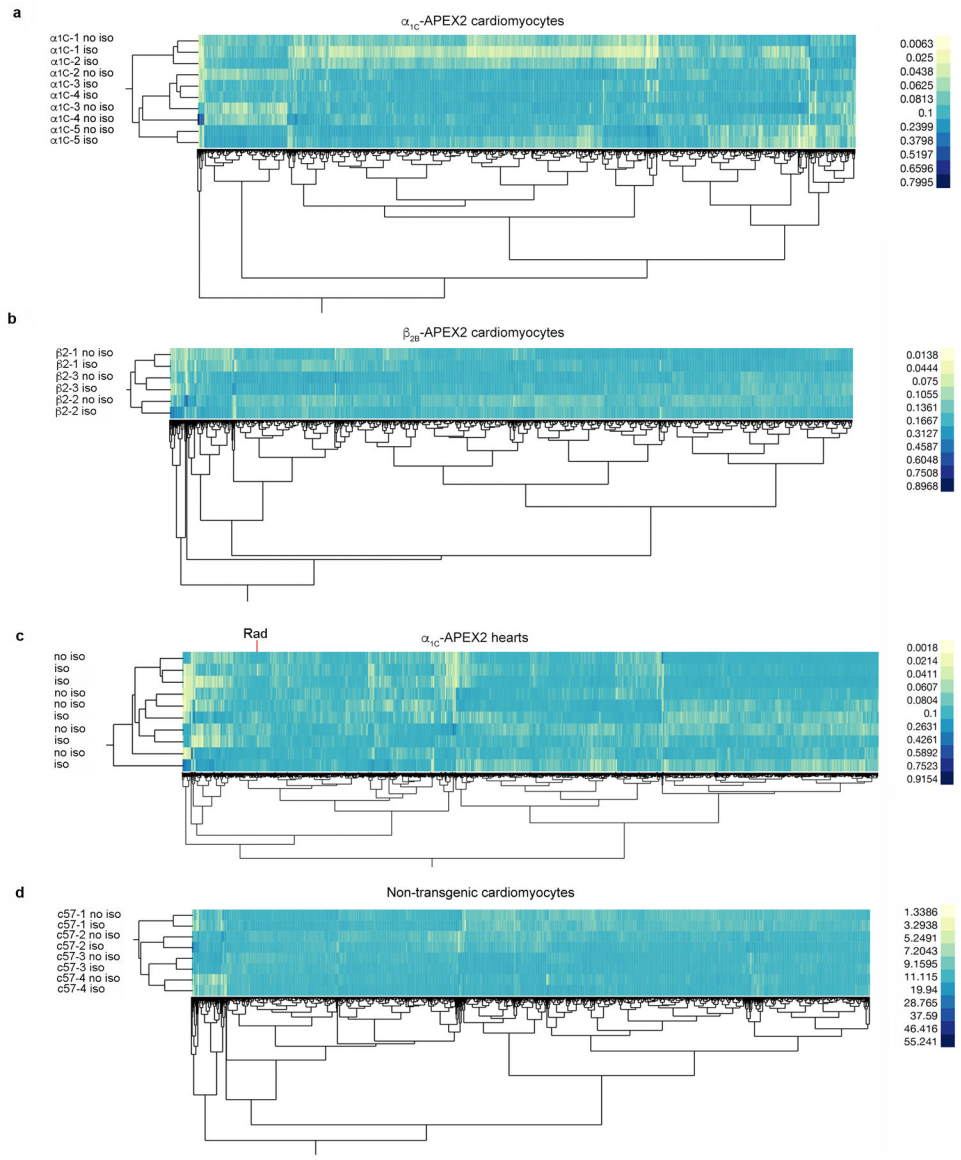

Extended Data Fig. 4. Two-way hierarchical clustering of scaled data from Fig. 2.

(a) Dendrogram showing two-way hierarchical clustering of scaled TMT signal to noise (s/n) data for streptavidin-purified proteins from α_{1C}-APEX2 expressing cardiomyocytes after vehicle or after isoproterenol stimulation. Scaled relative TMT protein quantification data for 1951 proteins from biological quintuplicate α_{1C}-APEX2. Clustering used Ward's minimum variance method. **(b)** Dendrogram showing two-way hierarchical clustering of scaled relative quantification data for 1936 proteins from biological triplicate β_{2B}-APEX2 experiments. Heterogeneity between cardiomyocyte preparations from different mice is apparent. **(c)** Dendrogram showing two-way hierarchical clustering of scaled relative quantification data for 2610 proteins from whole-organ α_{1C}-APEX without or with perfusion of isoproterenol. Prominent heterogeneity in relative protein quantification between hearts is apparent. Position of Rad is indicated by a red line. In this experiment, the individual hearts are not paired. **(d)** Dendrogram showing two-way hierarchical clustering of

Author Manuscript Author Manuscript Author Manuscript Author Manuscript

scaled TMT signal to noise (s/n) data from non-transgenic (NTG) cardiomyocytes under isoproterenol stimulation or with vehicle. Scaled data of 4622 quantified proteins from biological quadruplicate experiment are displayed. Pairing of samples is apparent.

Author Manuscript Author Manuscript Author Manuscript Author Manuscript

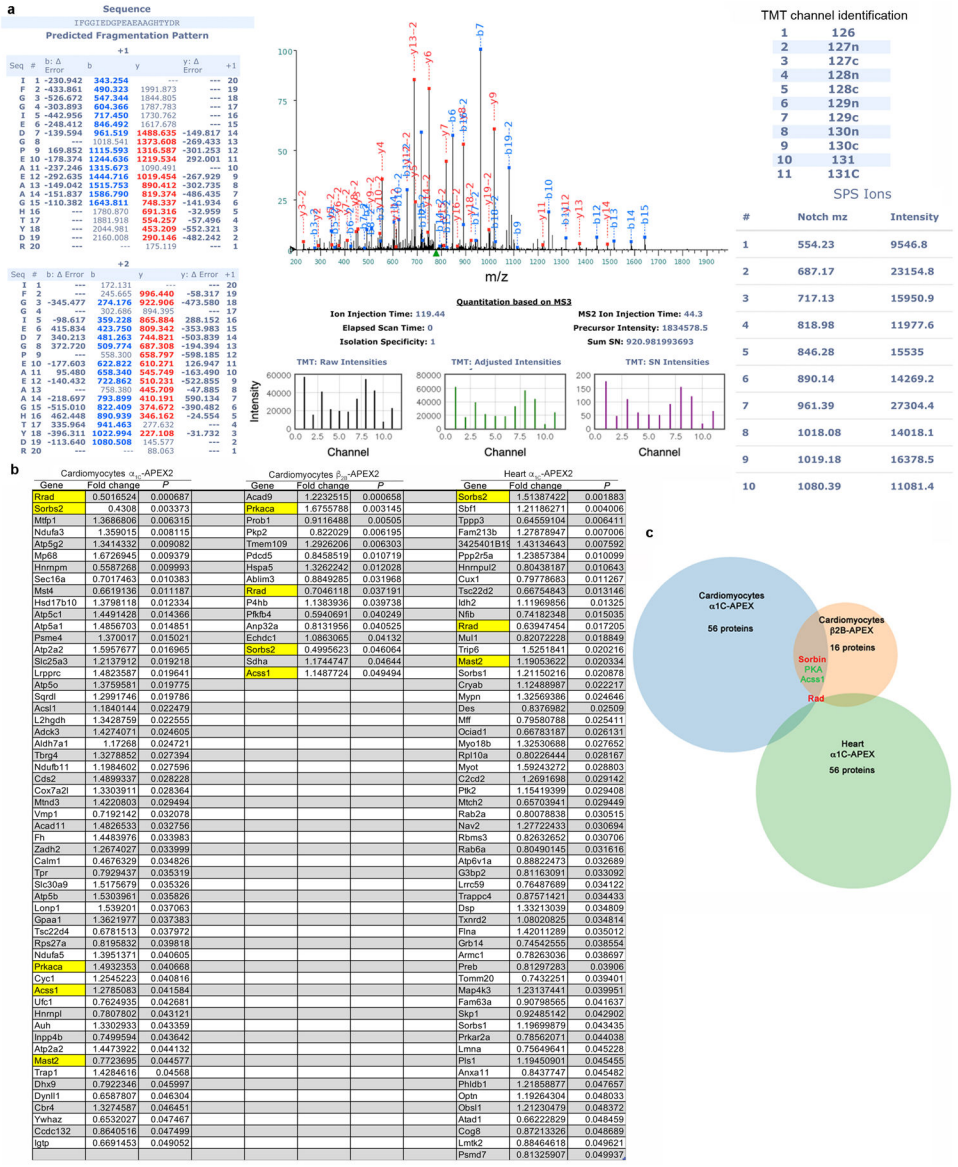

Extended Data Fig. 5. Isoproterenol-induced change in Rad detected by mass spectrometry.

(a) MS^2 spectrum and TMT quantification parameters of a Rad peptide changed upon isoproterenol treatment of murine hearts. The MS^2 spectrum used for identification of the peptide: IFGGIEDGPEAEAAGHTYDR mapping to Rad is displayed. y and b ion m/z identified in the spectrum and their deviation from theoretical m/z are displayed on the left. Precursor mass was measured as 778.71 Da with a charge of +3. Peptide modifications were +229.16 Da for TMT on the peptide N-terminus and lysine residues, +57.02 Da for cysteine alkylation and +15.99 for methionine oxidation. Ion injection times, isolation specificity, sum of signal to noise (SN) over all TMT channels, TMT raw intensities, adjusted intensities and final SN intensities used for relative quantification as well as SPS ion m/z are displayed. **(b)** Table showing gene names of proteins with $P < 0.05$ for the three approaches: cardiomyocytes isolated from α_{1C}-APEX and β_{2B}-APEX mice, and α_{1C}-APEX hearts. Yellow-highlighted genes are in common amongst groups, but note for Mast2, the fold-

Author Manuscript Author Manuscript Author Manuscript Author Manuscript

change is not consistent. D3Z0N2* is a single peptide with the sequence ESFDSQSLINNQSK and its abundance is reduced by isoproterenol-treatment in non-transgenic cardiomyocytes to 27% likely by post-translational modification (P =0.000002, see Fig. 3 and Supplementary Data Table 6). Data are mean fold-change for 5 pairs of biologically independent pairs of α_{1C}-APEX2 cardiomyocyte samples, 3 pairs of biologically independent pairs of β_{2B}-APEX cardiomyocyte samples, and 10 α_{1C}-APEX2 hearts, 5 without isoproterenol and 5 with isoproterenol. Non-adjusted unpaired two-tailed t-test. **(c)** Venn diagram of the data from (b). Proteins: Rad = Rrad; PKA catalytic subunit= Prkaca; Acss1 = acyl-CoA synthetase short chain family member 1. Rad is the only protein consistently changed amongst the three approaches.

Author Manuscript Author Manuscript Author Manuscript Author Manuscript

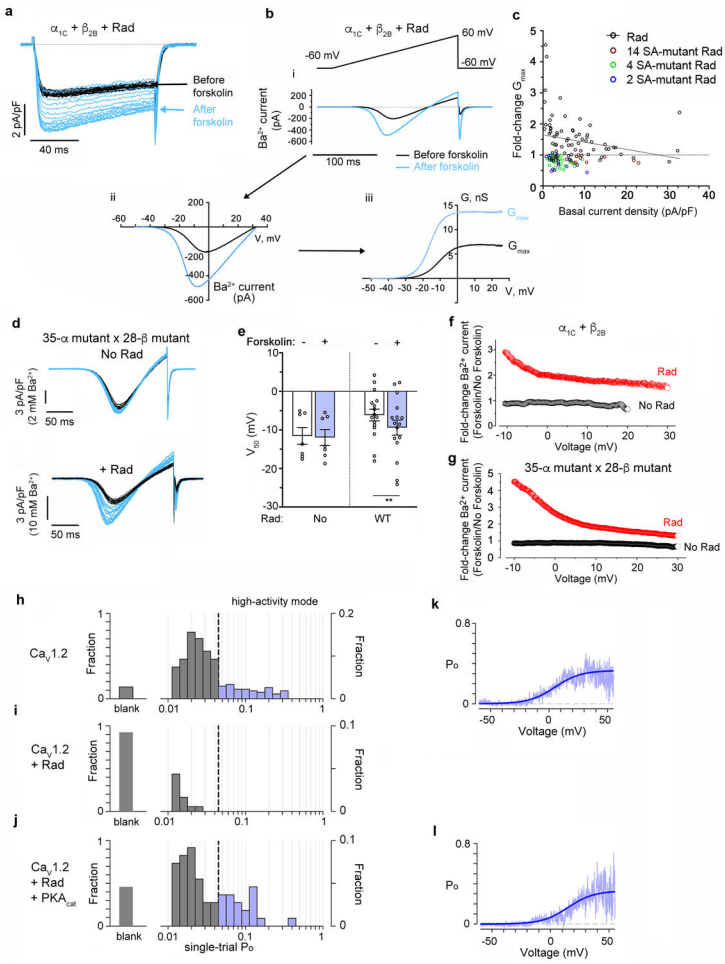

Extended Data Fig. 6. Rad is required for Forskolin-induced activation of heterologously expressed $Ca_V1.2$ channels.

(a) Exemplar whole-cell $Ca_V1.2$ currents elicited from step depolarizations recorded from HEK293T cells expressing Rad. Pulses every 10-s before (black traces) and during Forskolin (blue traces). Representative of at least 10 cells. **(b)** Methodology used for generating G/V curves. i. Upper: 200-ms voltage ramp from −60 mV to + 60 mV was applied every 10-s. Lower: Current traces – average of 3 traces before Forskolin (black) and 3 traces after Forskolin (blue). ii. Conversion of time scale to applied voltage. iii. Convert to G-V relationship. (G). Fold-change was calculated at G_{max}. **(c)** Graph of Forskolin-induced fold-change in current stratified by basal current density. **(d)** Exemplar traces of Ba^{2+} currents in absence and presence of Rad elicited by voltage ramp every 10-s. Black traces before and blue traces after Forskolin. no Rad:7 cells; Rad:16 cells. **(e)** Boltzmann function parameter V_{50}. Mean ± SEM. ** P <0.01 by paired two-tailed t-test. n= 7, 16, left to right. **(f-g)** Graphs of ratio of current after Forskolin to current before Forskolin for cells transfected without and with Rad. Representative of analyses for 3 cells for each condition. **(h-l)** The distribution of sweep-by-sweep average P_O (single trial P_O). (h) In absence of Rad, sweeps with no openings or blank sweeps are rare (10%), while most sweeps exhibit either intermediate-high levels of openings. (k) Pale blue lines are conditional P_o-voltage relationship obtained for sweeps exhibiting high activity. Blue line is Boltzmann fit. (i)

Fraction of blank sweeps is increased with expression of Rad. (j) If PKA catalytic domain is also co-expressed with Rad, the fraction of blank sweeps is reduced and there is a resurgence of the high activity mode. (l) Same as (k) but with Rad and PKA expression.

Author Manuscript Author Manuscript Author Manuscript Author Manuscript

Author Manuscript Author Manuscript Author Manuscript Author Manuscript

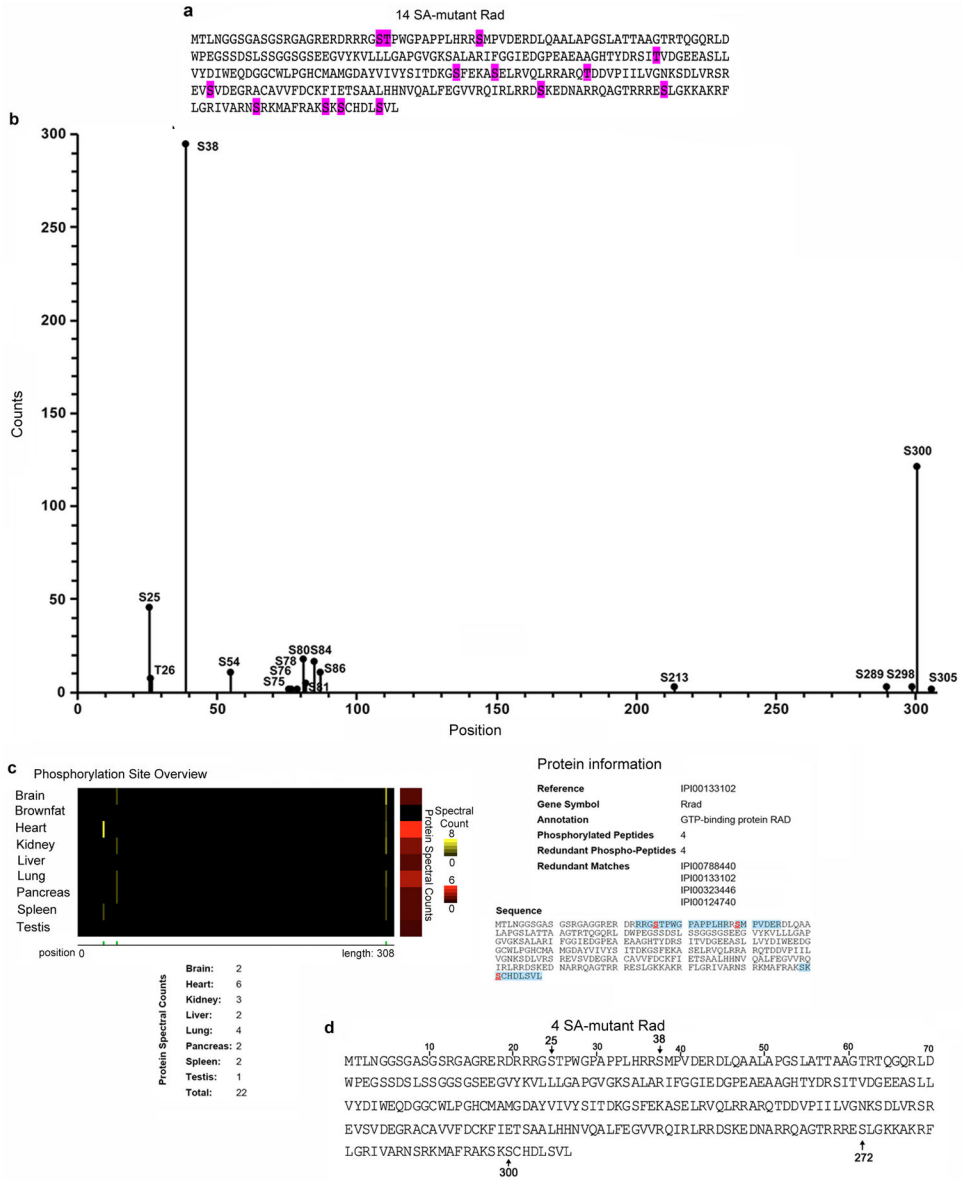

Extended Data Fig. 7. PKA phosphorylation sites in mouse Rad.

(a) Serine/threonine residues (purple-highlighted) mutated to alanine in the 14-SA mutant. **(b)** Mass spectrometry identification of phosphorylated residues on Rad enriched with an anti-GFP nanobody matrix from HEK cells expressing GFP-Rad and treated with forskolin. The number of spectral counts is plotted against the position of the phosphorylated amino acids in Rad. 534 aggregated phosphopeptides were detected from two independent experiments. **(c)** The database entry of phosphorylation sites identified previously in Rad is displayed. The highest level of Rad phosphorylation was detected in the heart. Peptides with phosphorylated Ser residues (bold, red) on positions 25, 38 and 300 (mapped to Rad expression constructs used in this study) were detected. (https://phosphomouse.hms.harvard.edu/site_view.php?ref=IPI00133102). **(d)** Serine residues mutated to alanine in 4-SA mutant indicated by arrows.

Author Manuscript Author Manuscript Author Manuscript Author Manuscript

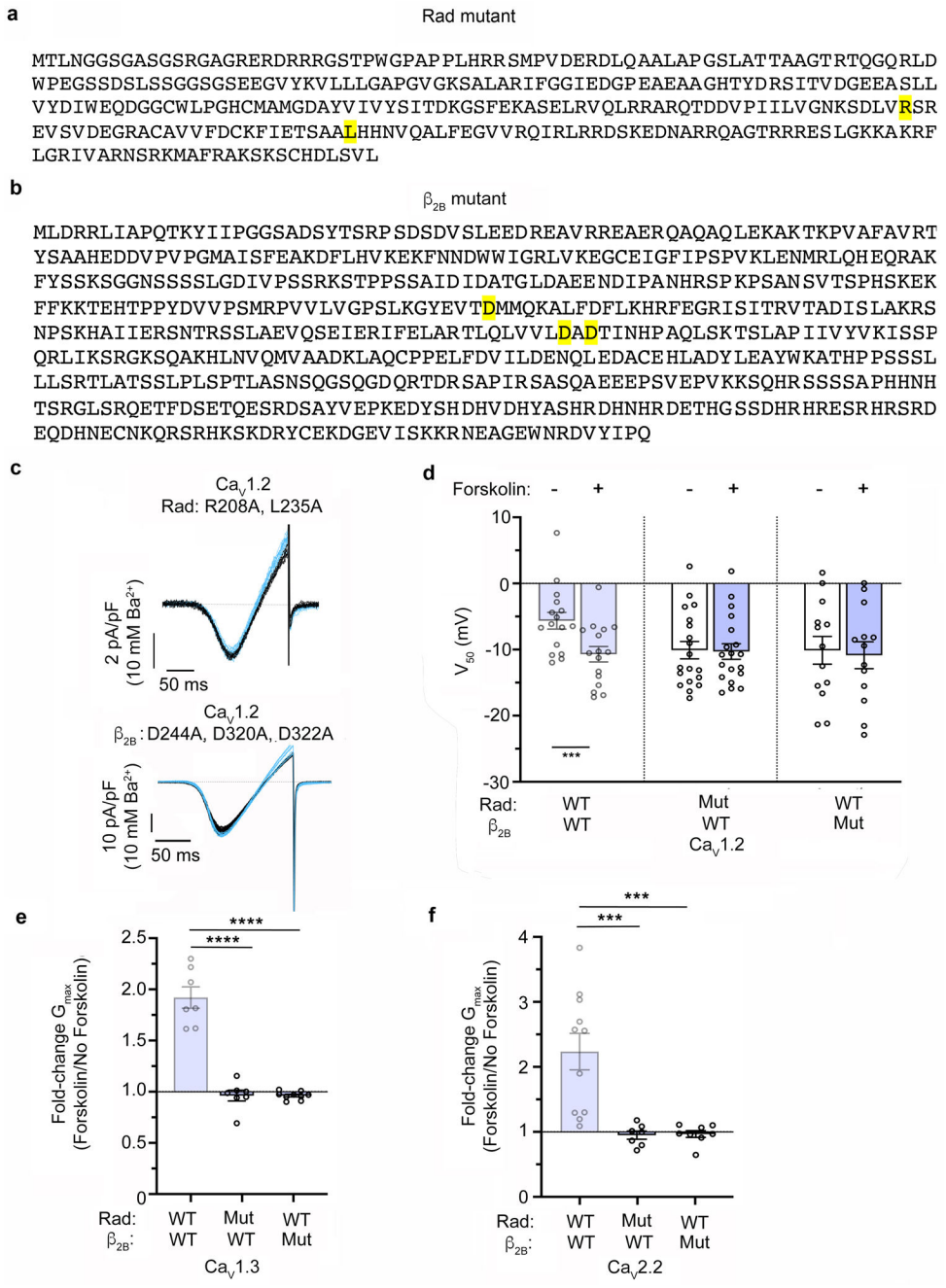

Extended Data Fig. 8. Binding of Rad and β_{2B} is required for regulation of Forskolin-induced stimulation of voltage-gated Ca^{2+} channels.

(a) Alanine substitutions of Rad at residues R208 and L235 (yellow-highlighted), and **(b)** alanine substitutions at residues D244, D320 and D322 (yellow-highlighted) of β_{2B} were created to attenuate Rad binding to β as described previously [28,29]. **(c)** Ba^{2+} current of $Ca_V1.2$ channels elicited by voltage ramp every 10 s from −60 mV to +60 mV over 200 ms. Black traces before and blue traces after Forskolin. Representative of 20 and 15 cells, from top to bottom. **(d)** Boltzmann function parameter V_{50}. Mean ± SEM. ** P <0.001 by paired two-tailed t-test. Data for WT Rad is same as Fig. 3h. Specific P values can be found in the

Author Manuscript Author Manuscript Author Manuscript Author Manuscript

Source Data associated with this figure. N= 16, 19, 13, from left to right. **(e)** Fold-change (Forskolin vs. No Forskolin) in G_{max}. Mean ± SEM. $P < 0.0001$ by one-way ANOVA; **** $P < 0.0001$ by Dunnett's test. Data for WT Rad and WT β_{2B} is same as Fig. 4e. n= 7, 7, 9 cells, from left to right. **(f)** Fold-change (forskolin vs. no forskolin) in G_{max}. Mean ± SEM. $P < 0.001$ by one-way ANOVA; *** $P < 0.001$ by Dunnett's test. Data for WT Rad and WT β_{2B} is same as Fig 4h. n= 11, 7, 8 cells, from left to right.

Author Manuscript Author Manuscript Author Manuscript Author Manuscript

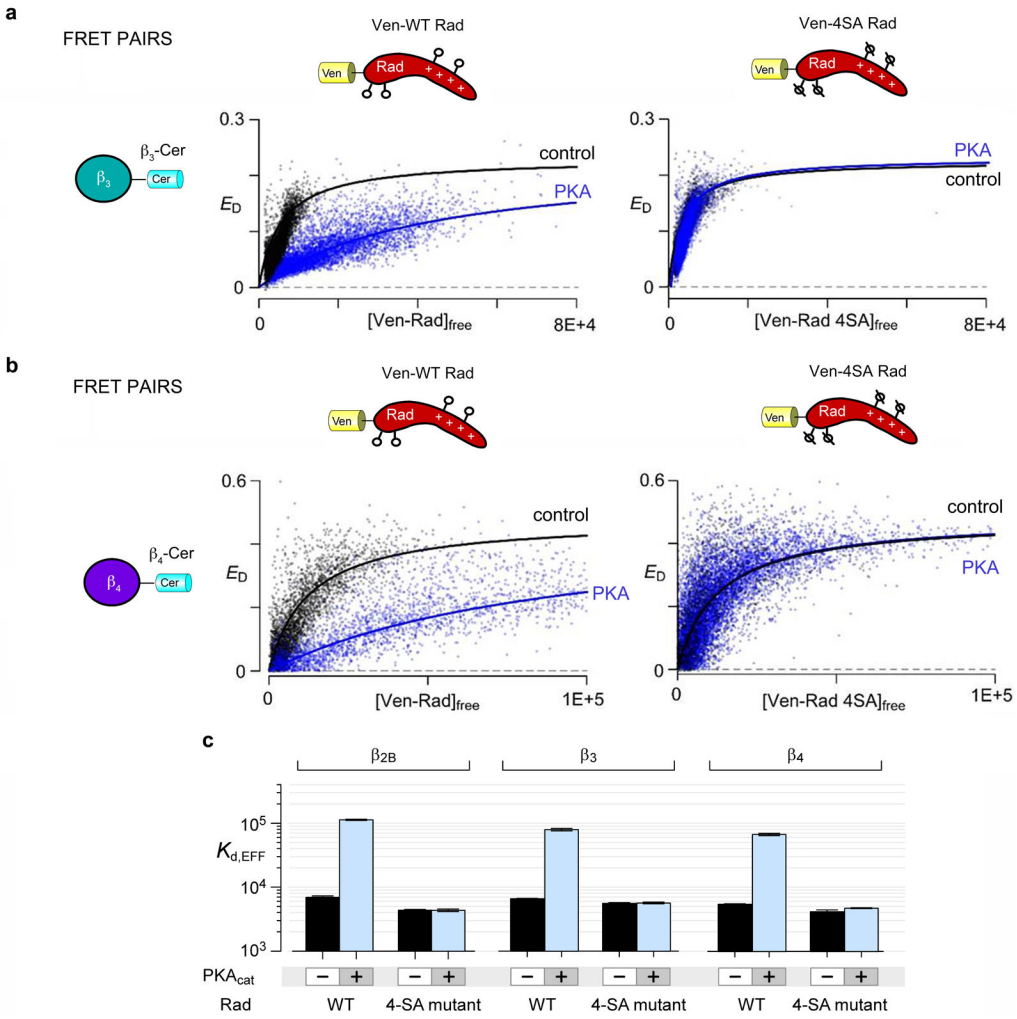

Extended Data Fig. 9. Phosphorylation-dependent dissociation of Rad and β_3 and β_4 subunits.

(a-b) FRET 2-hybrid binding isotherms were determined for Cerulean (Cer)-tagged β_3 and β_4, and N-terminal Venus (Ven)-tagged WT or 4-SA mutant Rad. FRET efficiency (E_D) is plotted against the free concentration Ven-WT or Ven-4SA-mutant Rad. Solid line fits a 1:1 binding isotherm. Co-expression of the PKA catalytic subunit weakened binding in WT Rad-expressing cells, but not 4-SA mutant Rad-expressing cells. (c) Bar graph summarizing mean $K_{d,EFF}$ for β_{2B}, β_3 and β_4, and WT and 4-SA mutant Rad, expressed without and with catalytic PKA subunit. Mean ± 95% confidence intervals (CI). The error bars on the $K_{d,EFF}$ are a 95%-CI for the pooled non-linear fits based on the Jacobians computed. The sample size for each condition is 1,580-10,364 cells acquired via two independent transfections and then pooled. The distribution of data in this graph is reflected in Fig. 4b-c, and in (a) and (b) of this figure.

Author Manuscript Author Manuscript Author Manuscript Author Manuscript

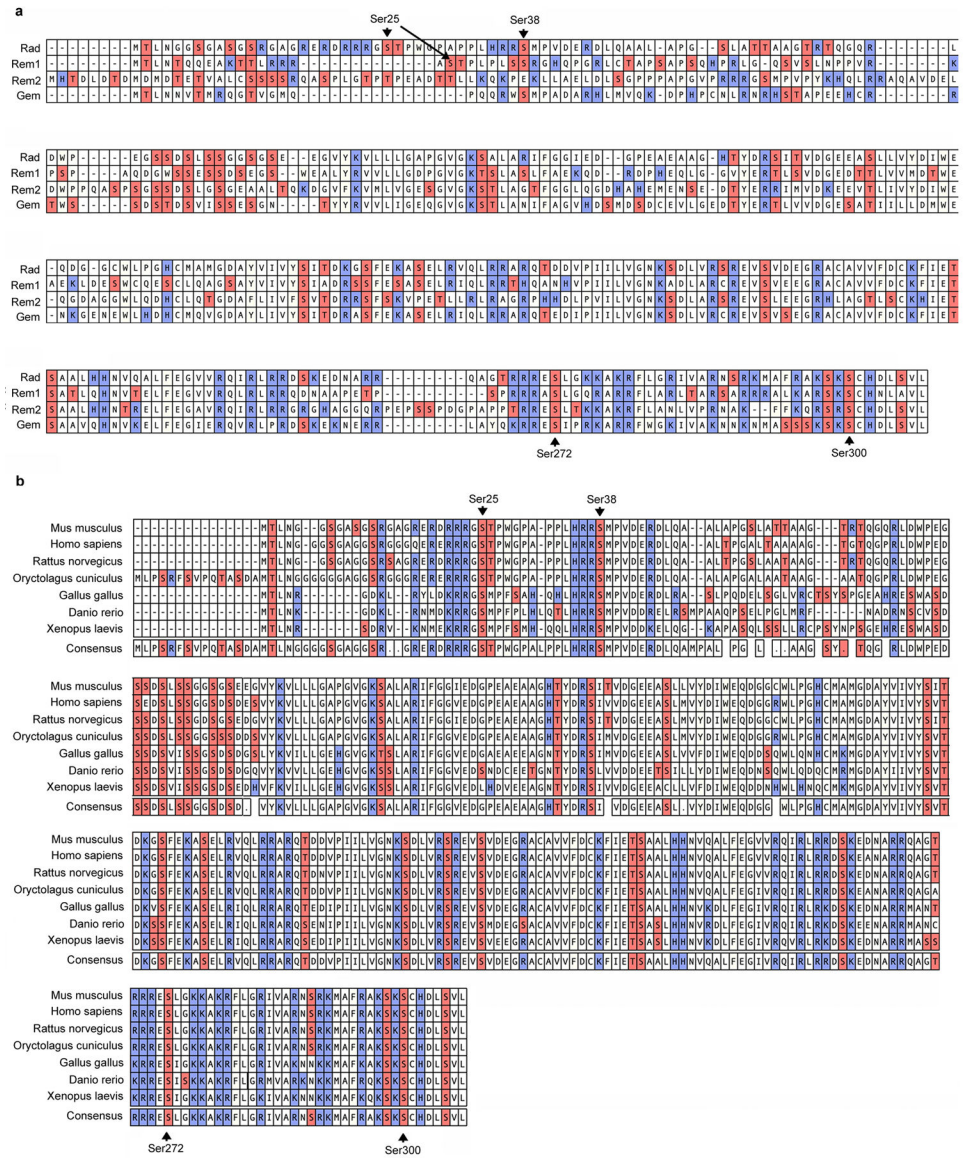

Extended Data Fig. 10. ClustalW alignment of Rad sequences and RGK GTPases.

(a) Conserved phosphorylation sites for mouse Ser^{25}, Ser^{38}, Ser^{272} and Ser^{300} are shown. Blue highlights basic amino acids (Arg, Lys and His), and red highlights Ser and Thr. **(b)** Phosphorylation sites for mouse Rad Ser^{25}, Ser^{38}, Ser^{272} and Ser^{300} are indicated (arrows). The C-terminal phosphorylation sites are conserved. The equivalent of Ser^{25} phosphorylation site is conserved in Rem1. The equivalent of Ser^{38} phosphorylation site is probably conserved in Gem. Blue highlights basic amino acids (Arg, Lys and His), and red highlights Ser and Thr.

Supplementary Material

Refer to Web version on PubMed Central for supplementary material.

Author Manuscript Author Manuscript Author Manuscript Author Manuscript

Acknowledgements

We thank Arthur Karlin for helpful discussions and editing the manuscript, Brian Soda for creating the cell model illustration, and Gary A. Bradshaw for technical assistance. This publication was supported by NIH R01 HL113136, R01 HL121253, and R01 HL146149, and by the National Center for Advancing Translational Sciences UL1TR001873. These studies used the resources of the Herbert Irving Comprehensive Cancer Center Flow Cytometry Shared Resources funded in part through Center Grant P30CA013696. Images were collected (and analyzed) in the Confocal and Specialized Microscopy Shared Resource of the Herbert Irving Comprehensive Cancer Center at Columbia University, supported by NIH grant #P30 CA013696 (National Cancer Institute). Arianne Papa was supported by T32 HL120826 and NSF DGE – 1644869. Daniel Roybal was supported by T32 HL120826 and F31 HL142178. Jared Kushner was supported by T32 HL007343 and the Glorney-Raisbeck Fellowship from the NY Academy of Medicine, and Jessica Hennessey was supported by T32 HL007854. The content is solely the responsibility of the authors and does not necessarily represent the official views of the NIH.

References:

1. Cachelin AB, de Peyer JE, Kokubun S & Reuter H Ca2+ channel modulation by 8-bromocyclic AMP in cultured heart cells. Nature 304, 462–464 (1983). [PubMed: 6308462]
2. Reuter H & Scholz H The regulation of the calcium conductance of cardiac muscle by adrenaline. J Physiol 264, 49–62 (1977). [PubMed: 839456]
3. Hartzell HC, Mery PF, Fischmeister R & Szabo G Sympathetic regulation of cardiac calcium current is due exclusively to cAMP-dependent phosphorylation. Nature 351, 573–576, doi: 10.1038/351573a0 (1991). [PubMed: 1710784]
4. Tsien RW, Giles W & Greengard P Cyclic AMP mediates the effects of adrenaline on cardiac purkinje fibres. Nat New Biol 240, 181–183 (1972). [PubMed: 4343950]
5. Hung V et al. Spatially resolved proteomic mapping in living cells with the engineered peroxidase APEX2. Nat Protoc 11, 456–475, doi:10.1038/nprot.2016.018 (2016). [PubMed: 26866790]
6. Rhee HW et al. Proteomic mapping of mitochondria in living cells via spatially restricted enzymatic tagging. Science 339, 1328–1331, doi:10.1126/science.1230593 (2013). [PubMed: 23371551]
7. Paek J et al. Multidimensional Tracking of GPCR Signaling via Peroxidase-Catalyzed Proximity Labeling. Cell 169, 338–349 e311, doi:10.1016/j.cell.2017.03.028 (2017). [PubMed: 28388415]
8. Beguin P et al. Regulation of Ca2+ channel expression at the cell surface by the small G-protein kir/Gem. Nature 411, 701–706, doi:10.1038/35079621 (2001). [PubMed: 11395774]
9. Finlin BS, Crump SM, Satin J & Andres DA Regulation of voltage-gated calcium channel activity by the Rem and Rad GTPases. Proc Natl Acad Sci U S A 100, 14469–14474, doi:10.1073/pnas.2437756100 (2003). [PubMed: 14623965]
10. De Jongh KS et al. Specific phosphorylation of a site in the full-length form of the alpha 1 subunit of the cardiac L-type calcium channel by adenosine 3',5'-cyclic monophosphate-dependent protein kinase. Biochemistry 35, 10392–10402, doi:10.1021/bi953023c (1996). [PubMed: 8756695]
11. Fuller MD, Emrick MA, Sadilek M, Scheuer T & Catterall WA Molecular mechanism of calcium channel regulation in the fight-or-flight response. Sci Signal 3, ra70, doi:10.1126/scisignal.2001152 (2010). [PubMed: 20876873]
12. Gerhardstein BL, Puri TS, Chien AJ & Hosey MM Identification of the sites phosphorylated by cyclic AMP-dependent protein kinase on the beta 2 subunit of L-type voltage-dependent calcium channels. Biochemistry 38, 10361–10370, doi:10.1021/bi990896o (1999). [PubMed: 10441130]
13. Ganesan AN, Maack C, Johns DC, Sidor A & O'Rourke B Beta-adrenergic stimulation of L-type Ca2+ channels in cardiac myocytes requires the distal carboxyl terminus of alpha1C but not serine 1928. Circ Res 98, e11–18, doi:10.1161/01.RES.0000202692.23001.e2 (2006). [PubMed: 16397147]
14. Lemke T et al. Unchanged beta-adrenergic stimulation of cardiac L-type calcium channels in Ca v 1.2 phosphorylation site S1928A mutant mice. J Biol Chem 283, 34738–34744, doi:10.1074/jbc.M804981200 (2008). [PubMed: 18829456]
15. Brandmayr J et al. Deletion of the C-terminal phosphorylation sites in the cardiac beta-subunit does not affect the basic beta-adrenergic response of the heart and the Ca(v)1.2 channel. J Biol Chem 287, 22584–22592, doi:10.1074/jbc.M112.366484 (2012). [PubMed: 22589548]

Author Manuscript Author Manuscript Author Manuscript Author Manuscript

16. Yang L et al. beta-adrenergic regulation of the L-type Ca2+ channel does not require phosphorylation of alpha1C Ser1700. Circ Res 113, 871–880, doi:10.1161/CIRCRESAHA.113.301926 (2013). [PubMed: 23825359]
17. Yang L et al. Cardiac CaV1.2 channels require beta subunits for beta-adrenergic-mediated modulation but not trafficking. J Clin Invest 129, 647–658, doi:10.1172/JCI123878 (2019). [PubMed: 30422117]
18. Martell JD et al. Engineered ascorbate peroxidase as a genetically encoded reporter for electron microscopy. Nat Biotechnol 30, 1143–1148, doi:10.1038/nbt.2375 (2012). [PubMed: 23086203]
19. Lobingier BT et al. An Approach to Spatiotemporally Resolve Protein Interaction Networks in Living Cells. Cell 169, 350–360 e312, doi:10.1016/j.cell.2017.03.022 (2017). [PubMed: 28388416]
20. Moyers JS, Zhu J & Kahn CR Effects of phosphorylation on function of the Rad GTPase. Biochem J 333 (Pt 3), 609–614 (1998). [PubMed: 9677319]
21. Manning JR et al. Rad GTPase deletion increases L-type calcium channel current leading to increased cardiac contraction. J Am Heart Assoc 2, e000459, doi:10.1161/JAHA.113.000459 (2013). [PubMed: 24334906]
22. Levitan BM et al. Rad-deletion Phenocopies Tonic Sympathetic Stimulation of the Heart. J Cardiovasc Transl Res 9, 432–444, doi:10.1007/s12265-016-9716-y (2016). [PubMed: 27798760]
23. Wang G et al. Rad as a novel regulator of excitation-contraction coupling and beta-adrenergic signaling in heart. Circ Res 106, 317–327, doi:10.1161/CIRCRESAHA.109.208272 (2010). [PubMed: 19926875]
24. Xu X, Marx SO & Colecraft HM Molecular mechanisms, and selective pharmacological rescue, of Rem-inhibited CaV1.2 channels in heart. Circ Res 107, 620–630, doi:10.1161/CIRCRESAHA.110.224717 (2010). [PubMed: 20616312]
25. Bean BP, Nowycky MC & Tsien RW Beta-adrenergic modulation of calcium channels in frog ventricular heart cells. Nature 307, 371–375 (1984). [PubMed: 6320002]
26. Huttlin EL et al. A tissue-specific atlas of mouse protein phosphorylation and expression. Cell 143, 1174–1189, doi:10.1016/j.cell.2010.12.001 (2010). [PubMed: 21183079]
27. Heo WD et al. PI(3,4,5)P3 and PI(4,5)P2 lipids target proteins with polybasic clusters to the plasma membrane. Science 314, 1458–1461, doi:10.1126/science.1134389 (2006). [PubMed: 17095657]
28. Yang T, Puckerin A & Colecraft HM Distinct RGK GTPases differentially use alpha1- and auxiliary beta-binding-dependent mechanisms to inhibit CaV1.2/CaV2.2 channels. PLoS One 7, e37079, doi:10.1371/journal.pone.0037079 (2012). [PubMed: 22590648]
29. Beguin P et al. RGK small GTP-binding proteins interact with the nucleotide kinase domain of Ca2+-channel beta-subunits via an uncommon effector binding domain. J Biol Chem 282, 11509–11520, doi:10.1074/jbc.M606423200 (2007). [PubMed: 17303572]
30. Lee SR, Sang L & Yue DT Uncovering Aberrant Mutant PKA Function with Flow Cytometric FRET. Cell Rep 14, 3019–3029, doi:10.1016/j.celrep.2016.02.077 (2016). [PubMed: 26997269]
31. Chang DD & Colecraft HM Rad and Rem are non-canonical G-proteins with respect to the regulatory role of guanine nucleotide binding in Ca(V)1.2 channel regulation. J Physiol 593, 5075–5090, doi:10.1113/JP270889 (2015). [PubMed: 26426338]
32. Mahapatra S, Marcantoni A, Zuccotti A, Carabelli V & Carbone E Equal sensitivity of Cav1.2 and Cav1.3 channels to the opposing modulations of PKA and PKG in mouse chromaffin cells. J Physiol 590, 5053–5073, doi:10.1113/jphysiol.2012.236729 (2012). [PubMed: 22826131]
33. Mangoni ME et al. Functional role of L-type Cav1.3 Ca2+ channels in cardiac pacemaker activity. Proc Natl Acad Sci U S A 100, 5543–5548, doi:10.1073/pnas.0935295100 (2003). [PubMed: 12700358]
34. Bailey MJ & Prehoda KE Establishment of Par-Polarized Cortical Domains via Phosphoregulated Membrane Motifs. Dev Cell 35, 199–210, doi:10.1016/j.devcel.2015.09.016 (2015). [PubMed: 26481050]
35. Kranias EG Regulation of Ca2+ transport by cyclic 3’,5’-AMP-dependent and calcium-calmodulin-dependent phosphorylation of cardiac sarcoplasmic reticulum. Biochim Biophys Acta 844, 193–199, doi:10.1016/0167-4889(85)90090-4 (1985). [PubMed: 2982423]

Author Manuscript Author Manuscript Author Manuscript Author Manuscript

36. Qian H et al. Phosphorylation of Ser1928 mediates the enhanced activity of the L-type Ca2+ channel Cav1.2 by the beta2-adrenergic receptor in neurons. Sci Signal 10, doi:10.1126/scisignal.aaf9659 (2017).
37. Nystoriak MA et al. Ser1928 phosphorylation by PKA stimulates the L-type Ca2+ channel CaV1.2 and vasoconstriction during acute hyperglycemia and diabetes. Sci Signal 10, doi:10.1126/scisignal.aaf9647 (2017).
38. Folci A et al. Molecular mimicking of C-terminal phosphorylation tunes the surface dynamics of CaV1.2 calcium channels in hippocampal neurons. J Biol Chem 293, 1040–1053, doi:10.1074/jbc.M117.799585 (2018). [PubMed: 29180451]
39. Ito DW et al. beta-adrenergic-mediated dynamic augmentation of sarcolemmal CaV 1.2 clustering and co-operativity in ventricular myocytes. J Physiol 597, 2139–2162, doi:10.1113/JP277283 (2019). [PubMed: 30714156]
40. Chai S et al. Physiological genomics identifies genetic modifiers of long QT syndrome type 2 severity. J Clin Invest 128, 1043–1056, doi:10.1172/JCI94996 (2018). [PubMed: 29431731]
41. Belbachir N et al. RRAD mutation causes electrical and cytoskeletal defects in cardiomyocytes derived from a familial case of Brugada syndrome. Eur Heart J 40, 3081–3094, doi:10.1093/eurheartj/ehz308 (2019). [PubMed: 31114854]
42. Katchman A et al. Proteolytic cleavage and PKA phosphorylation of alpha1C subunit are not required for adrenergic regulation of CaV1.2 in the heart. Proc Natl Acad Sci U S A 114, 9194–9199, doi:10.1073/pnas.1706054114 (2017). [PubMed: 28784807]
43. Yang L et al. The PDZ motif of the alpha1C subunit is not required for surface trafficking and adrenergic modulation of CaV1.2 channel in the heart. J Biol Chem 290, 2166–2174, doi:10.1074/jbc.M114.602508 (2015). [PubMed: 25505241]
44. Sanbe A et al. Reengineering inducible cardiac-specific transgenesis with an attenuated myosin heavy chain promoter. Circ Res 92, 609–616, doi:10.1161/01.RES.0000065442.64694.9F (2003). [PubMed: 12623879]
45. Hambleton M et al. Inducible and myocyte-specific inhibition of PKCalpha enhances cardiac contractility and protects against infarction-induced heart failure. Am J Physiol Heart Circ Physiol 293, H3768–3771, doi:10.1152/ajpheart.00486.2007 (2007). [PubMed: 17921332]
46. He M, Bodi I, Mikala G & Schwartz A Motif III S5 of L-type calcium channels is involved in the dihydropyridine binding site. A combined radioligand binding and electrophysiological study. J Biol Chem 272, 2629–2633 (1997). [PubMed: 9006896]
47. Hockerman GH et al. Construction of a high-affinity receptor site for dihydropyridine agonists and antagonists by single amino acid substitutions in a non-L-type Ca2+ channel. Proc Natl Acad Sci U S A 94, 14906–14911 (1997). [PubMed: 9405712]
48. Lam SS et al. Directed evolution of APEX2 for electron microscopy and proximity labeling. Nat Methods 12, 51–54, doi:10.1038/nmeth.3179 (2015). [PubMed: 25419960]
49. Bramson HN, Kaiser ET & Mildvan AS Mechanistic studies of cAMP-dependent protein kinase action. CRC Crit Rev Biochem 15, 93–124 (1984). [PubMed: 6365450]
50. Kemp BE, Graves DJ, Benjamini E & Krebs EG Role of multiple basic residues in determining the substrate specificity of cyclic AMP-dependent protein kinase. J Biol Chem 252, 4888–4894 (1977). [PubMed: 194899]
51. Moore MJ, Adams JA & Taylor SS Structural basis for peptide binding in protein kinase A. Role of glutamic acid 203 and tyrosine 204 in the peptide-positioning loop. J Biol Chem 278, 10613–10618, doi:10.1074/jbc.M210807200 (2003). [PubMed: 12499371]
52. Feramisco JR, Glass DB & Krebs EG Optimal spatial requirements for the location of basic residues in peptide substrates for the cyclic AMP-dependent protein kinase. J Biol Chem 255, 4240–4245 (1980). [PubMed: 6246116]
53. Songyang Z et al. Use of an oriented peptide library to determine the optimal substrates of protein kinases. Curr Biol 4, 973–982 (1994). [PubMed: 7874496]
54. Neuberger G, Schneider G & Eisenhaber F pkaPS: prediction of protein kinase A phosphorylation sites with the simplified kinase-substrate binding model. Biol Direct 2, 1, doi:10.1186/1745-6150-2-1 (2007). [PubMed: 17222345]

Author Manuscript Author Manuscript Author Manuscript Author Manuscript

55. Iakoucheva LM et al. The importance of intrinsic disorder for protein phosphorylation. Nucleic Acids Res 32, 1037–1049, doi:10.1093/nar/gkh253 (2004). [PubMed: 14960716]
56. Zhou FF, Xue Y, Chen GL & Yao X GPS: a novel group-based phosphorylation predicting and scoring method. Biochem Biophys Res Commun 325, 1443–1448, doi:10.1016/j.bbrc.2004.11.001 (2004). [PubMed: 15555589]
57. Blom N, Gammeltoft S & Brunak S Sequence and structure-based prediction of eukaryotic protein phosphorylation sites. J Mol Biol 294, 1351–1362, doi:10.1006/jmbi.1999.3310 (1999). [PubMed: 10600390]
58. Obenauer JC, Cantley LC & Yaffe MB Scansite 2.0: Proteome-wide prediction of cell signaling interactions using short sequence motifs. Nucleic Acids Res 31, 3635–3641 (2003). [PubMed: 12824383]
59. Valencik ML & McDonald JA Codon optimization markedly improves doxycycline regulated gene expression in the mouse heart. Transgenic Res 10, 269–275 (2001). [PubMed: 11437283]
60. Wan E et al. Aberrant sodium influx causes cardiomyopathy and atrial fibrillation in mice. J Clin Invest 126, 112–122, doi:10.1172/JCI84669 (2016). [PubMed: 26595809]
61. Yang L, Katchman A, Morrow JP, Doshi D & Marx SO Cardiac L-type calcium channel (Cav1.2) associates with gamma subunits. FASEB J 25, 928–936, doi:10.1096/fj.10-172353 (2011). [PubMed: 21127204]
62. Yang L et al. Protein kinase C isoforms differentially phosphorylate Ca(v)1.2 alpha(1c). Biochemistry 48, 6674–6683, doi:10.1021/bi900322a (2009). [PubMed: 19527072]
63. Marx SO et al. PKA phosphorylation dissociates FKBP12.6 from the calcium release channel (ryanodine receptor): defective regulation in failing hearts. Cell 101, 365–376 (2000). [PubMed: 10830164]
64. Kalocsay M APEX Peroxidase-Catalyzed Proximity Labeling and Multiplexed Quantitative Proteomics. Methods Mol Biol 2008, 41–55, doi:10.1007/978-1-4939-9537-0_4 (2019). [PubMed: 31124087]
65. McAlister GC et al. MultiNotch MS3 enables accurate, sensitive, and multiplexed detection of differential expression across cancer cell line proteomes. Anal Chem 86, 7150–7158, doi:10.1021/ac502040v (2014). [PubMed: 24927332]
66. Beausoleil SA, Villen J, Gerber SA, Rush J & Gygi SP A probability-based approach for high-throughput protein phosphorylation analysis and site localization. Nat Biotechnol 24, 1285–1292, doi:10.1038/nbt1240 (2006). [PubMed: 16964243]
67. Paulo JA et al. Quantitative mass spectrometry-based multiplexing compares the abundance of 5000 S. cerevisiae proteins across 10 carbon sources. J Proteomics 148, 85–93, doi:10.1016/j.jprot.2016.07.005 (2016). [PubMed: 27432472]
68. Perez-Riverol Y et al. The PRIDE database and related tools and resources in 2019: improving support for quantification data. Nucleic Acids Res 47, D442–D450, doi:10.1093/nar/gky1106 (2019). [PubMed: 30395289]
69. Deutsch EW et al. The ProteomeXchange consortium in 2017: supporting the cultural change in proteomics public data deposition. Nucleic Acids Res 45, D1100–D1106, doi:10.1093/nar/gkw936 (2017). [PubMed: 27924013]
70. Maere S, Heymans K & Kuiper M BiNGO: a Cytoscape plugin to assess overrepresentation of gene ontology categories in biological networks. Bioinformatics 21, 3448–3449, doi:10.1093/bioinformatics/bti551 (2005). [PubMed: 15972284]
71. Tay LH et al. Nanodomain Ca(2)(+) of Ca(2)(+) channels detected by a tethered genetically encoded Ca(2)(+) sensor. Nat Commun 3, 778, doi:10.1038/ncomms1777 (2012). [PubMed: 22491326]
72. Adams PJ, Ben-Johny M, Dick IE, Inoue T & Yue DT Apocalmodulin itself promotes ion channel opening and Ca(2+) regulation. Cell 159, 608–622, doi:10.1016/j.cell.2014.09.047 (2014). [PubMed: 25417111]

Author Manuscript Author Manuscript Author Manuscript Author Manuscript

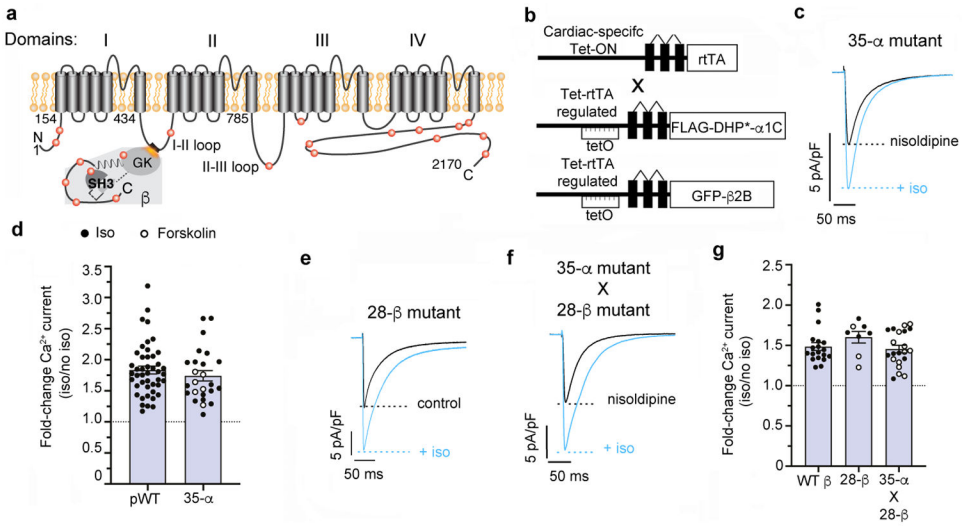

Fig. 1. Phosphorylation of α_{1C} and β subunits by PKA is not required for β-adrenergic regulation of $Ca_V1.2$.

(a) Schematic of rabbit cardiac α_{1C} and β subunits. Red dots indicate putative PKA phosphorylation sites. **(b)** Schematic of binary transgene system. The expression of reverse tetracycline-controlled transactivator (rtTA) is driven by the cardiac-specific α-myosin heavy chain promoter. The cDNAs for FLAG-DHP-resistant (DHP*) α_{1C} or GFP-β_{2B} were ligated behind 7 tandem *tetO* sequences. **(c)** Exemplar whole-cell $Ca_V1.2$ currents of 35-mutant α_{1C} transgenic mice cardiomyocytes in nisoldipine before (black trace) and after isoproterenol (blue trace). Representative of 25 experiments. **(d)** Fold-change of peak DHP-resistant Ca^{2+} current at 0 mV caused by isoproterenol or forskolin. Mean ± SEM. P=0.39 by unpaired two-tailed t-test. n= 45 cardiomyocytes from 5 mice, n = 25 cardiomyocytes from 5 mice. **(e-f)** Exemplar whole-cell $Ca_V1.2$ currents of GFP-tagged-28-mutant β_{2B} transgenic mice cardiomyocytes, and 35-mutant α_{1C} X 28-mutant β_{2B} transgenic mice cardiomyocytes. Representative of 8 and 22 independent experiments respectively. **(g)** Fold-change in peak Ca^{2+} current caused by isoproterenol or forskolin for cardiomyocytes isolated from transgenic mice expressing GFP-tagged WT β_{2B} subunit [17], GFP-tagged 28-mutant β_{2B}, or both 35-mutant α_{1C} and GFP-tagged 28-mutant β_{2B}. Mean ± SEM. P=0.27 by one way-ANOVA. n= 19, 8, 21 cardiomyocytes from 4, 4, 3 mice, from left to right.

Author Manuscript Author Manuscript Author Manuscript Author Manuscript

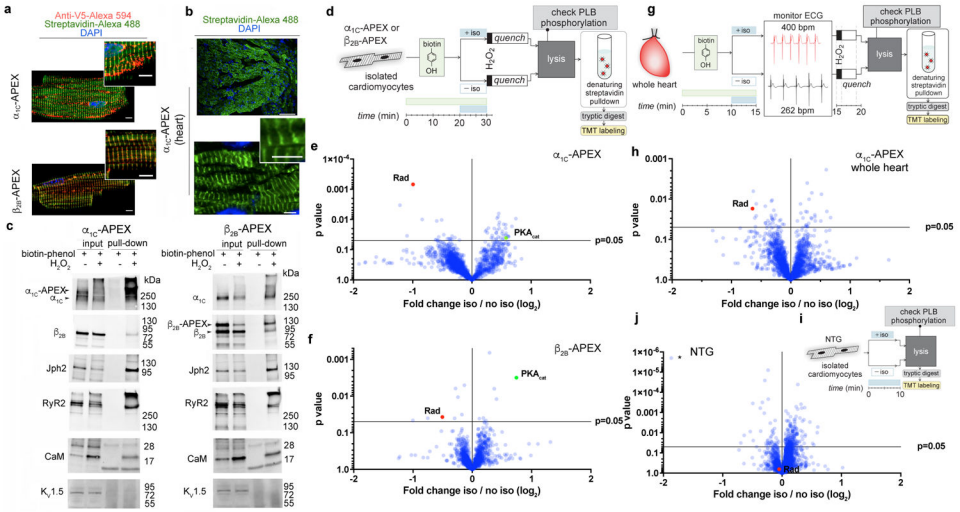

Fig. 2. Changes in $Ca_V1.2$ subdomain proteome upon β-adrenergic agonist activation of PKA signaling in heart.

(a) Immunofluorescence of isolated α_{1C}-APEX2 and β_{2B}-APEX2 cardiomyocytes exposed to biotin-phenol and H_2O_2. Representative of 13 and 8 cardiomyocytes from 2 and 3 mice respectively. Scale bar = 5 μm. **(b)** Immunofluorescence of tissue sections of Langendorff-perfused α_{1C}-APEX2 heart. Scale bars: upper −100 μm; lower − 5 μm; lower inset− 5 μm. Representative of 10 sections from 2 mice. **(c)** Immunoblots of biotin-labeled proteins from α_{1C}-APEX2 and β_{2B}-APEX2 mice cardiomyocytes. In contrast to $Ca_V1.2$ subunits, RyR2, Jph2 and CaM, $K_V1.5$ channels were not detected in streptavidin-pulldown. Blots representative of 3 independent experiments. **(d)** Schematic of workflow for isolated cardiomyocytes. **(e)** Volcano plot of fold-change for relative protein quantification by TMT mass spectrometry of α_{1C}-APEX2 samples. Data shown are means for 5 pairs of biologically-independent samples. Non-adjusted unpaired two-tailed t-test. Rad (red dot) is reduced by 50% and PKA catalytic subunit (green dot) is increased by 50%. **(f)** Same as (e) except cardiomyocytes from β_{2B}-APEX2 mice. Data shown are means for 3 pairs of biologically independent samples. Rad is reduced by 30% and PKA catalytic subunit is increased by 68%. **(g)** Schematic of protein labeling and workflow for Langendorff-perfused α_{1C}-APEX2 mice hearts. bpm= beats per minute. **(h)** Same as (d) except proteins from α_{1C}-APEX2 whole heart samples. Data shown are means for 10 hearts, 5 without isoproterenol and 5 with isoproterenol. Rad is reduced by 36% **(i)** Schematic of workflow for isolated cardiomyocytes from non-transgenic (NTG) mice. **(j)** Same as (e) except proteins isolated from non-transgenic (NTG) mice cardiomyocytes without biotinylation or pull-down. * single peptide ESFDSQSLINNQSK. Data shown are means for 4 pairs of biologically-independent samples. Rad (red dot) in whole heart is unchanged by isoproterenol. For source gel data, see Supplementary Fig. 1.

Author Manuscript Author Manuscript Author Manuscript Author Manuscript

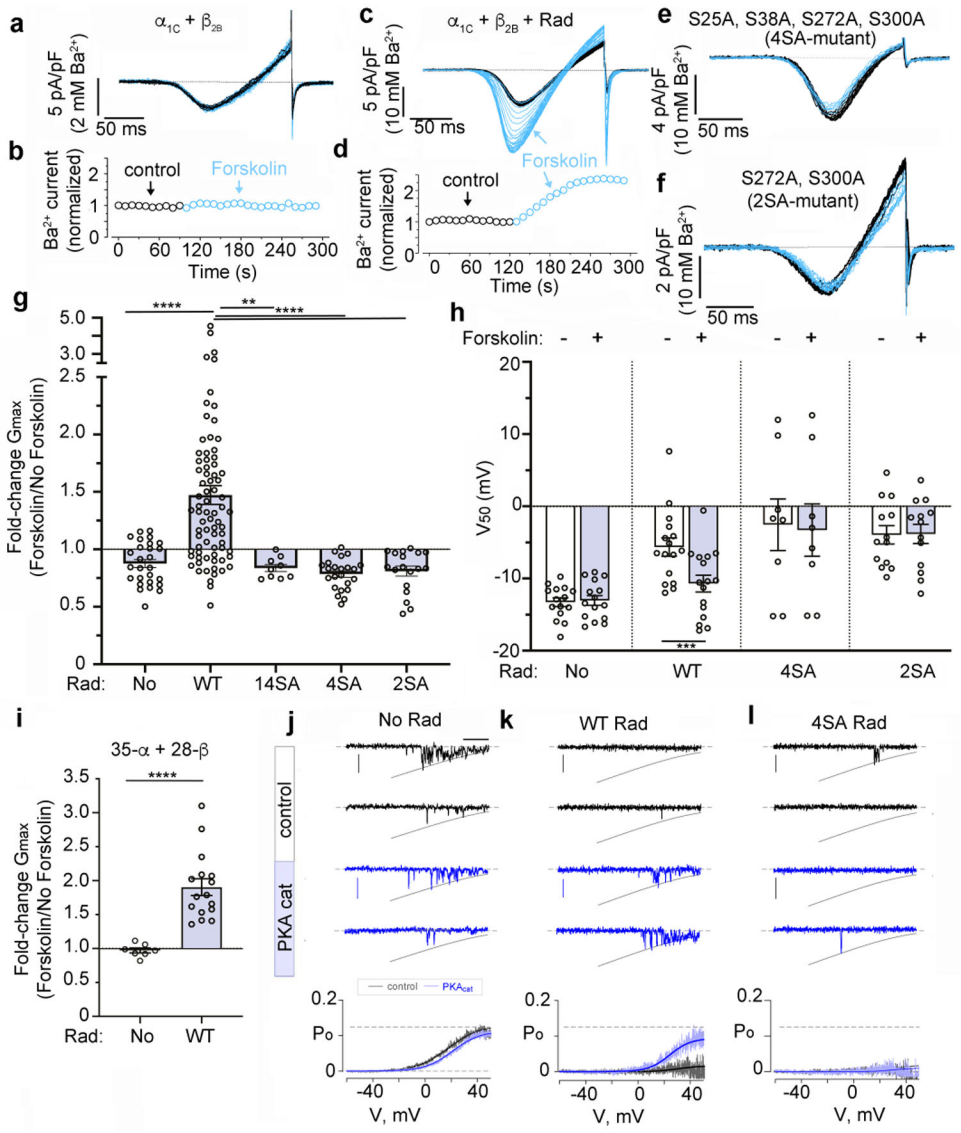

Fig. 3. Phosphorylation of Rad is required for cAMP-PKA activation of $Ca_V1.2$.

(a, c, e, f) Ba^{2+} current elicited by voltage ramp every 10s. Black traces before and blue traces after forskolin. Representative of 15,16, 8 and 13 cells, respectively. **(b, d)** Diary plot of normalized Ba^{2+} current amplitude at 0 mV. Representative of 15 and 16 cells. **(g)** Fold-change in maximum conductance (G_{max}) induced by forskolin. Mean ± SEM. $P < 0.0001$ by one-way ANOVA; ** $P < 0.01$, **** $P < 0.0001$ by Tukey's test. n= 27, 76, 9, 23, 18 cells, from left to right. Specific P values can be found in the Source Data associated with this figure. **(h)** Boltzmann function parameter V_{50}. Mean ± SEM. *** $P < 0.001$ by two-tailed paired t-test. n= 15, 16, 8, 13, from left to right. **(i)** Fold-change in G_{max} induced by forskolin in absence and presence of Rad. Mean ± SEM. **** $P < 0.0001$ by unpaired two-tailed t-test. n= 7, 16, left to right. **(j-l)** The top rows display stochastic records, where channel closures are zero-current portions of the trace (horizontal gray lines) and openings are downward deflections to the open level (slanted gray lines). Bottom row: pale blue and gray lines are average P_O-V relationship from multiple cells. Blue and black lines are

Author Manuscript Author Manuscript Author Manuscript Author Manuscript

Boltzmann fits. In all experiments, α_{1C} and β_{2B} were expressed in HEK cells with no Rad (j), WT Rad (k), or 4 SA-mutant Rad (l), in the absence or presence of exogenous PKA catalytic subunit. Dashed line is maximal P_O for control of α_{1C} + β_{2B} without Rad. Scale bars: 1 pA and 25 ms. Control, n= 10; Control + PKA, n=5; Rad, n=5; Rad + PKA, n=8; 4SA mutant Rad, n=6, 4SA mutant Rad + PKA, n=5.

Author Manuscript Author Manuscript Author Manuscript Author Manuscript

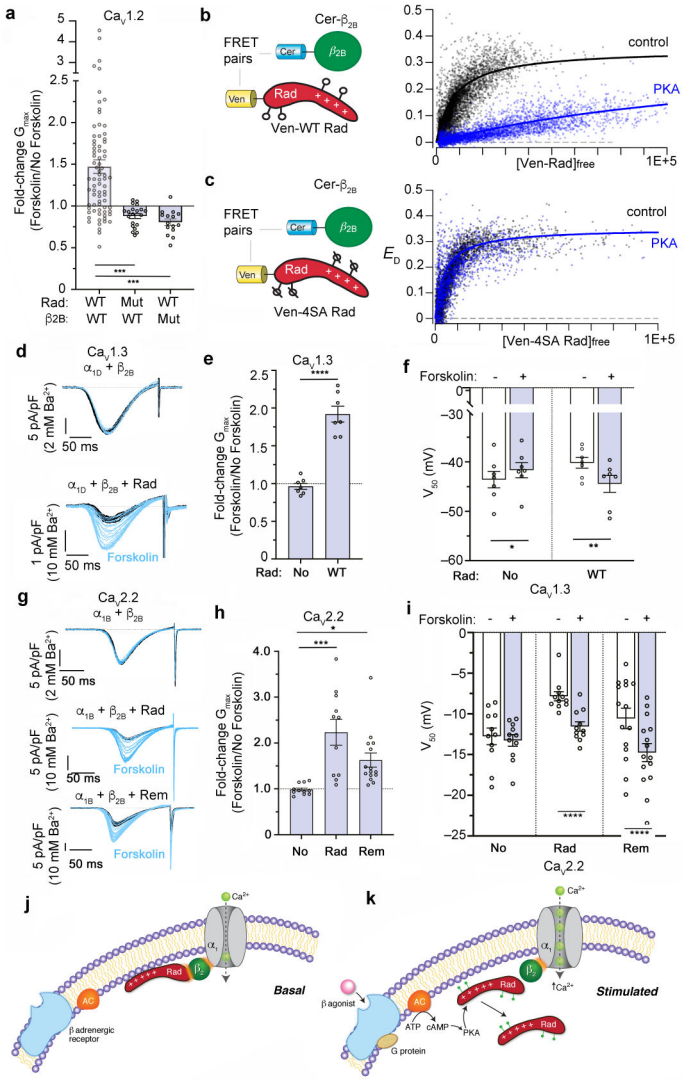

Fig. 4. RGK GTPases confer adrenergic regulation to $Ca_V1.2$, $Ca_V1.3$ and $Ca_V2.2$ channels via binding to β.

(**a**) Fold-change in G_{max}. Mean ± SEM. $P < 0.0001$ by one-way ANOVA; *** $P < 0.001$ by Dunnett's test. Data for Rad is same as Fig. 3g. n= 76, 20, 15, left to right. Specific P values can be found in the Source Data associated with this figure. **(b-c)** FRET efficiency (E_D) is plotted against the free concentration Ven-WT (b) or Ven-4SA-mutant Rad (c). Solid line fits a 1:1 binding isotherm. **(d)** Ba^{2+} current of $Ca_V1.3$ channels without or with expression of Rad elicited by voltage ramp every 10 s. Black traces before and blue traces after forskolin. No Rad, Rad: 7 cells each. **(e)** Fold-change in G_{max}. Mean ± SEM. **** P <0.0001 by unpaired two-tailed t-test. n= 7 for both. **(f)** Boltzmann function parameter V_{50}. Mean ± SEM. * $P < 0.05$; ** $P < 0.01$ by paired two-tailed t-test. n=7 for no Rad and Rad. **(g)** Ba^{2+} current of $Ca_V2.2$ channels without or with expression of Rad or Rem elicited by voltage ramp every 10 s. Black traces before and blue traces after forskolin. Representative of 11,11,15, top to bottom. **(h)** Fold-change in G_{max}. Mean ± SEM. $P < 0.001$ by one-way ANOVA; **** $P < 0.0001$, *** $P < 0.001$, * $P < 0.05$ by Dunnett's test. n= 11, 11, 15, left to

Author Manuscript Author Manuscript Author Manuscript Author Manuscript

right. **(i)** Boltzmann function parameter V_{50}. Mean ± SEM. **** P<0.001 by paired two-tailed t-test; n=11, 11, 15, from left to right. **(j-k)** Proposed model of β-adrenergic regulation of Ca^{2+} channels. Basal state (j) and after (k) β-agonist-induced activation of PKA leads to PKA-phosphorylation of Rad causing dissociation of Rad from the $Ca_V1.2$ complex and subsequently increased Ca^{2+} influx. AC: adenylyl cyclase.